PROCESSING AND MECHANICAL PROPERTIES OF Ti_2AlC REINFORCED WITH ALUMINA FIBERS

A Thesis

by

KWONGUK JEON

Submitted to the Office of Graduate Studies of
Texas A&M University
in partial fulfillment of the requirements for the degree of

MASTER OF SCIENCE

August 2011

Major Subject: Mechanical Engineering

PROCESSING AND MECHANICAL PROPERTIES OF Ti_2AlC REINFORCED WITH ALUMINA FIBERS

A Thesis

by

KWONGUK JEON

Submitted to the Office of Graduate Studies of
Texas A&M University
in partial fulfillment of the requirements for the degree of

MASTER OF SCIENCE

Approved by:

Chair of Committee,	Miladin Radovic
Committee Members,	Ibrahim Karaman
	Sean M. McDeavitt
Head of Department,	Dennis O'Neal

August 2011

Major Subject: Mechanical Engineering

ABSTRACT

Processing and Mechanical Properties of Ti_2AlC Reinforced with Alumina Fibers.

(August 2011)

Kwonguk Jeon, B.E., Korea Military Academy

Chair of Advisory Committee: Dr. Miladin Radovic

The fabrication and mechanical properties of Ti_2AlC composites reinforced with the alumina oxide fibers, such as Nextel^{TM} 720 and ALBF1, were described in this thesis. Alumina fibers and Ti_2AlC powders were dispersed in the water and slip cast in the molds to form green bodies. Sedimentation test were carried out to optimize pH of the slurry. It was found that suspensions prepared with PAA as a dispersant and has an excellent stability in the pH range of 4 ~ 5. Composite green bodies were densified by pressureless sintering or hot isotatic pressing (HIP) at different temperatures. The microstructure of fabricated samples was characterized by X-ray diffraction (XRD), scanning electron microscopy (SEM) equipped with energy dispersive X-ray spectroscopy (EDS), and porosimetry. It was found out that HIPing at 1300 ^{o}C for 4 hrs at 100 MPa results in almost fully dense composites with majority phases being alumina fibers and Ti_2AlC. However, fully dense Ti_2AlC composites could not be obtained by the pressurless sintering, even at temperature as high as 1400 ^{o}C at which reaction between Ti_2AlC and Nextel^{TM} 720 was observed.

The double torsion (DT) tests were carried out at room temperature to measure the fracture toughness of the HIPed pure and 5vol% alumina fiber reinforced Ti_2AlC. DT results showed increase in the fracture toughness of Ti_2AlC reinforcing with Nextel^{TM} 720 alumina fibers. However, fracture toughness of the samples reinforced with ALBF1 was lower than that of pure Ti_2AlC because of the low relative densities of those composites. SEM study of the fracture surfaces after DT tests showed that toughening mechanisms by crack bridging and fiber pull outs at the crack tip are operative in all reinforced samples. In addition, elastic moduli of HIPed Ti_2AlC measured by Resonant Ultrasound Spectroscopy (RUS) do not show significant change due to reinforcement with alumina fibers, while the Vickers hardness of composites was found to be larger for Ti_2AlC reinforced with Nextel^{TM} 720 and lower for the samples reinforced with ALBF1.

DEDICATION

To my lovely wife, Minjeong Ha, and all of my family members

who have always been there for me

ACKNOWLEDGEMENTS

I would like to thank my advisor, Dr. Miladin Radovic, not only for academic guidance and advice but also for the support he has given me in last two years. Sincere thanks are due to Dr. Ibrahim Karaman and Dr. Sean M. McDeavitt for their valuable recommendations and consideration as committee members.

I also appreciate the big favors from Dr. Sandip Basu of helping me in many areas. I would like to thank Rogelio Benitez for doing RUS analysis.

TABLE OF CONTENTS

LIST OF FIGURES

FIGURE Page

FIGURE Page

LIST OF TABLES

1. INTRODUCTION

1.1 MAX Phases

In the early 1960s, W. Jeitschko, H. Nowotny and F. Benesovsky discovered a new family of ternary carbides and nitrides of early transition metals. After many years, they finally successfully processed a large number of new ternary compounds in the form of thin films, which they named H-phases. After successful synthesis of bulk H-phases by Barsoum and his group in the late 1990s, this family of materials has been usually referred to as MAX phases.

The MAX phases are ternary carbides and nitrides with chemical formula $M_{n+1}AX_n$ (n=1, 2 and 3), where M denotes an early transition metal, A is an A-group element (mostly IIIA and IVA element) and X is either C or N. MAX phases elements are shown in Figure 1.

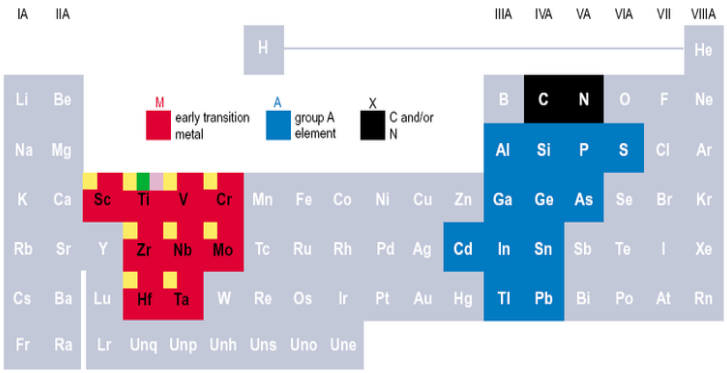

Figure 1. MAX phases elements in periodic table [1].

This thesis follows the style of *Science Direct.*

These phases have hexagonal structure with $M_{n+1}X_n$ layers interleaved with layers of pure A-group element [2]. The structures of MAX phases phases are shown in Figure 2. X element is located in every second octrahedral site in $M_{n+1}X_n$ sublayers.

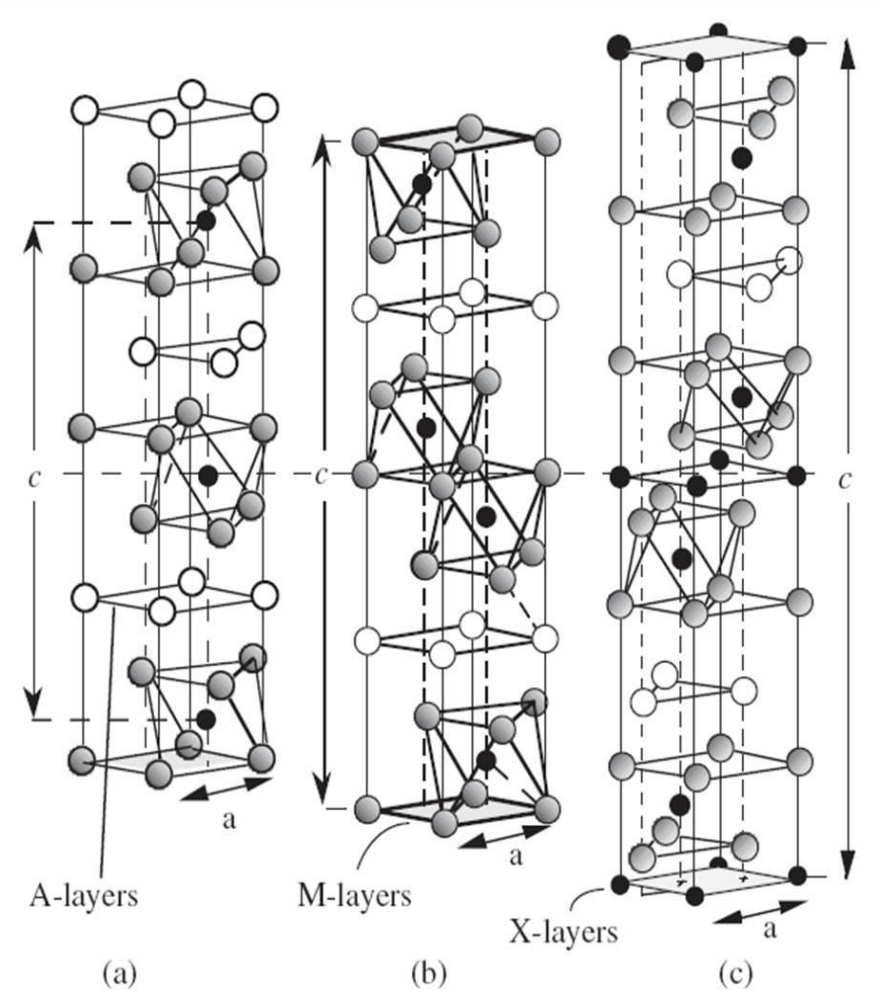

Figure 2. Structures of MAX phases (a) M_2AX, (b) M_3AX_2, (c) M_4AX_3 [3].

The A-group elements are located at the centers of trigonal prisms between M atoms, that are slightly larger than octahedral sites occupied by X element. $M_{n+1}AX_n$ phases

have 2, 3, and 4 layers of M respectively separated by the A-layers in the unit cells [3]. Up to date, approximately 60 phases have been found and most of them belong to 211 phase. Only 5 of 312 phase [4-7], and 7 of 413 phase [8-12] are known. Fruitful development of various synthesizing methods over the last 10 years has contributed to progress of the MAX phases. The known MAX phases are summarized in Table 1.

Table 1. The known MAX phases.

M_2AX (48)	Ti_2AlC, Ti_2AlN, Hf_2PbC, Cr_2GaC, V_2AsC, Ti_2InN, Nb_2AlC, $(Nb, Ti)_2AlC$, $Ti2AlN_{0.5}C_{0.5}$, Nb_2GaC, Nb_2AsC, Zr_2InN, Ti_2GeC, Cr_2AlC, Zr_2SC, Mo_2GaC, Ti_2CdC, Hf_2InN, Zr_2SnC, Ta_2AlC, Ti_2SC, Ta_2GaC, Sc_2InC, Hf_2SnN, Hf_2SnC, V_2AlC, Nb_2SC, Ti_2GaN, Ti_2InC, Ti_2TiC, Ti_2SnC, V_2PC, Hf_2SC, Cr_2GaN, Zr_2InC, Zr_2TiC, Nb_2SnC, Nb_2PC, Ti_2GaC, V_2GaN, Nb_2InC, Hf_2TiC, Zr_2PbC, Ti_2PbC, V_2GaC, V_2GeC, Hf_2InC, Zr_2TiN
M_3AX_2 (5)	Ti_3SiC_2, Ti_3GeC_2, Ti_3AlC_2, Ti_3SnC_2, Ta_3AlC_2
M_4AX_3 (7)	Ti_4AlN_3, Ti_4SiC_3, Ta_4AlC_3, Ti_4GaC_3, Nb_4AlC_3, Nb_4SiC_3, V_4AlC_3

The MAX phases have attracted attention in recent years because of their unique combination of ceramic and metallic properties. They are elastically stiff, have relatively low thermal expansion coefficients, good thermal and electrical conductivities, and are resistant to chemical attack [3, 13]. However, they are relatively soft and most readily machinable, not susceptible to thermal shock, and damage tolerant. Furthermore, some of the MAX phases are fatigue and creep or oxidation resistant [13]. These properties

can be useful in many applications, such as bearings, heating elements, nozzles, heat exchangers, tools for die pressing, turbine blades, etc [3].

1.2 Processing, Mechanical Properties, and Oxidation Resistance of Ti_2AlC

Among the MAX phases, Ti_2AlC is the good choice for high temperature structural applications. In 1963, W. Jeitschko et al. found that this MAX phase has a hexagonal structure with lattice parameters of a = 0.304 nm and c= 1.360 nm [14]. The crystal structure of Ti_2AlC is shown in Figure 3.

In sixties, Jeitschko et al. synthesized Ti_2AlC for the first time by sintering elemental powders for 150 h at 1000 ^oC [14]. After that, Ivchenko et al. [15] attempted to fabricate Ti_2AlC in two steps - first, bulk Ti_2AlC was prepared by sintering the powders and then ground to powders for subsequent sintering. From this method, the Ti_2AlC, with 90 ~ 92% density, was synthesized. Over two decades later, Barsoum et al. succeeded in fabrication of fully dense and high-purity bulk Ti_2AlC from Ti, Al_4C_3 and graphite powders by either reactive hot pressing (HP) at 1600 ^oC and 40 MPa for 4 hrs [16] or reactive hot isostatic pressing (HIP) at 1300 ^oC and 40 MPa for 30 h [17]. In 2003, Zhou et al. [18] obtained the bulk Ti_2AlC material with the high-purity by spark plasma sintering (SPS) of 2Ti / 1.2Al / C at 1100 ^oC and 30 MPa for 1 h. The temperature for SPS was lower than that for HP or HIP and the theoretical density of Ti_2AlC was 99.8 % [18]. Recently, combustion synthesis (SHS) has been used because this method can save time and lower energy requirement. Khoptiar et al. [19] applied

SHS to synthesize Ti_2AlC through peritectic reaction between liquid titanium aluminides and solid TiC_x [19]. The typical methods for the synthesis of Ti_2AlC are summarized in Table 2.

Table 2. Typical methods for the synthesis of Ti_2AlC [20].

Methods	Materials and conditions	Feature
HIP [17]	Ti / Al_4C_3 / C ; 1300 ^oC, 30 h, 40 MPa	Dense
HP [16]	Ti / Al_4C_3 / C; 1600 ^oC, 4 h, 40 MPa	Dense
SPS [18]	Ti / Al / C ; 1100 ^oC, 1 h, 30 MPa	Single-phase, Dense
SHS [19]	Ti / Al / C	Single-phase

Like other MAX phases, Ti_2AlC has good mechanical and electrical properties at

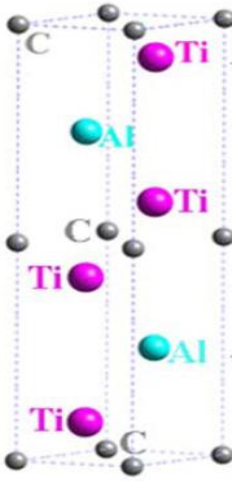

Figure 3. Crystal structure of Ti_2AlC [20].

high temperature. However, Ti_2AlC is the most lightweight and oxidation resistant among MAX phases [3] which is of crucial importance for high temperature structural applications.

The earliest oxidation study showed that oxidation behavior of Ti_2AlC occurs by the inward diffusion of oxygen and the outward diffusion of cations (Al^{3+}, Ti^{4+}) which form $(Ti_{1-y}Al_y)O_{2-y/2}$ oxide surface layer at the parabolic oxidation kinetics [21]. Sundberg et al. [22] showed that protective, dense, crack-free and stable alumina scales, forms on Ti_2AlC surfaces during oxidation at 1100 ^oC. In addition, they showed that oxide scales are thermal shock resistant and do not crack even after 8,000 thermal cycles up to 1350 ℃. Byeon et al. [23] measured the compressive residual stresses of alumina formed during oxidation of Ti_2AlC at 1000, 1200 and 1400 ℃ and found that the they are slightly compressive, thus contributing to the its stability and good adherence to the substrate. All of these studies showed that Ti_2AlC is the most oxidation resistant MAX phases and more oxidation resistant than most of the currently available alumina forming materials. The excellent oxidation resistance has been the most important attribute of Ti_2AlC that triggered interested of the research community in this compound as a potential candidate material for high temperature applications, such as heating elements, oxidation resistant films for coatings, cladding materials for nuclear applications, etc [20].

In all above mentioned applications, the mechanical properties are also of crucial importance, and thus several research groups reported on the mechanical properties of Ti_2AlC. The typical mechanical properties of Ti_2AlC are shown in Table 3.

Table 3. Typical mechanical properties of Ti_2AlC.

Vickers hardness (GPa)	Flexural strength (MPa)	Compressive strength (MPa)	Fracture toughness ($MPa \cdot m^{1/2}$)	BDTT (^oC)
4.5 [2], 2.8 [17]	275 [17]	763 [17], 540 [2]	6.5 [17]	1050 [17]

BDTT – brittle-to-ductile transition temperature

Ti_2AlC, similar to other MAX phase, although elastically quite stiff is machinable and dissipate significant amount of mechanical energy during the cycling loading even at room temperature [24]. The relative stiffness of Ti_2AlC is quite significant compared to other materials, because of its relatively low density. In addition, although Ti_2AlC and many other MAX phases have brittle to ductile transition between 1000 and 1100 ℃, their stiffness is not a strong function of the temperature [3]. For example, the shear modulus of Ti_2AlC is about 88% of its room temperature value at 1000 ℃ [25].

Additional imperative characteristic of all MAX phases, including Ti_2AlC is a presence of large number of mobile basal plane dislocation which explain why MAX phases are damage tolerant and fracture resistant [13]. The basal plane dislocations exist, glide and multiply in MAX phases, but they are confined only to the basal plane. Thus, dislocations are usually arranged in pileups, arrays or kink bands (KBs). Kink banks (KBs) suppress effectively delaminations and crack propagation along the basal planes making them quite fracture resistant when compared to other layered materials. Typical

delamination and kinking of the MAX phase (Ti_3SiC_2) are shown in Figure 4. Gilbert et al. [26] also showed that the stress to extend a crack in MAX phases rises with the crack extension because of delamination, kinking and extensive crack bridging when the crack is growing. In Figure 5, the crack is bridged by heavily deformed delaminations at the crack tip.

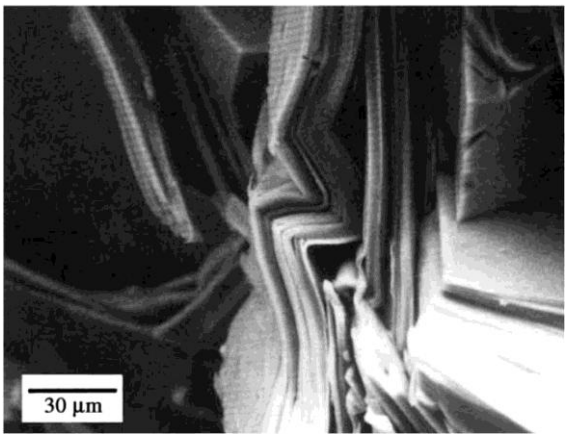

Figure 4. Typical delamination and kinking of Ti_3SiC_2 [13].

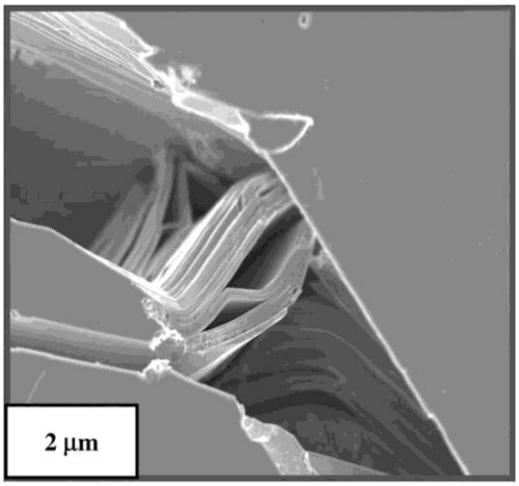

Figure 5. SEM image of a bridged crack in Ti_3SiC_2 microstructure [26].

1.3. Overview of Different Methods for Strengthening $Ti_{n+1}AlC_n$ Phases

Along with the research efforts to synthesize Ti_2AlC and characterize its properties, several studies reported on the attempts to reinforce Ti_2AlC with other ceramic materials in order to improve its high temperature mechanical properties. Among reinforcing ceramic materials, Al_2O_3 has been chosen frequently to enhance the properties of Ti_2AlC because previous oxidation studies showed good chemical compatibility of Al_2O_3 and Ti_2AlC. In addition, Al_2O_3 is considered a good reinforcing phase because of its high hardness, modulus and excellent chemical stability.

Hashimoto et al. [27] mixed Ti_2AlC (average grain size : 10 um) and 5 vol % Al_2O_3 (average grain size : 0.25 um, true density : 3.99 g/cm^3) by ball milling for 24 hrs. The mixture powder was cold-isostatically-pressed (CIP) at 100 MPa and then sintered for 2 hrs at 1400 ^oC in Ar. The result showed that the relative density and Vickers hardness increased by adding 5 vol % Al_2O_3 to Ti_2AlC. The experimental data are shown in Table 4.

Table 4. The mechanical properties of Ti_2AlC with and without Al_2O_3 after HPing at 1400 ^oC for 2 hrs in Ar [27].

	No additive	With additive (5 vol % Al_2O_3)
Relative density (%)	94.2	96.0
Vickers hardness (GPa)	2.8	3.5

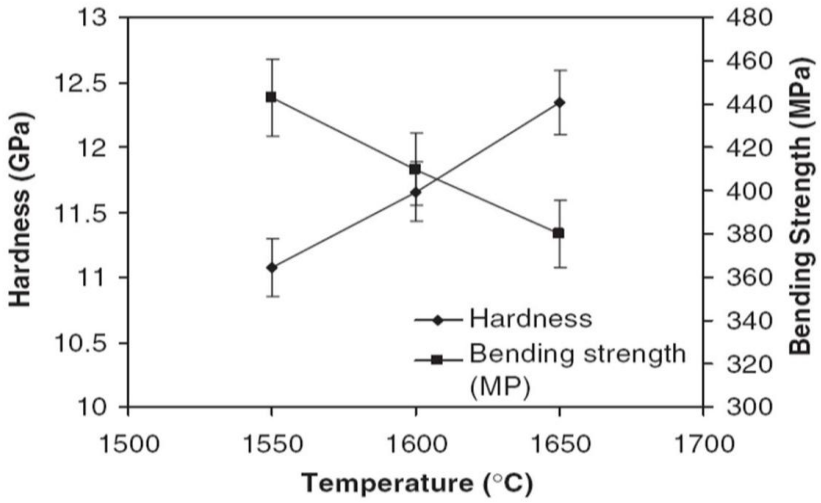

Figure 6. Hardness and bending strength of the Ti_2AlC composite as a function of sintering temperature [28].

Zhang et al. [28] reported on in situ synthesis of $Ti_2AlC/TiC/Al_2O_3$ composite with a composition of Ti_2AlC-20 vol % TiC - 35 vol % Al_2O_3 by cold pressing under 200 MPa and sintering at different temperature. They also showed that embedding Al_2O_3 particles with sizes of 0.5 ~ 15 um in a Ti_2AlC/TiC matrix affects significantly sintering process, as well as hardness and bending strength of the composites. The composites with the larger Al_2O_3 particles size required higher sintering temperatures. Also, as the size of Al_2O_3 particle increased, the average hardness of the composite increased to the ranges of 11 ~ 12.5 GPa, which is much higher than the hardness of the pure Ti_2AlC phase of 4 ~ 5 GPa [29]. This work demonstrated that Al_2O_3 particles and TiC grains, that have the hardness of approximately 16 GPa and 20 ~ 30 GPa, respectively, could reinforced the Ti_2AlC composite. On the other hand, the average bending strength of the composite showed decrease from 440 MPa to 380 MPa, with increasing in sintering

temperature and correspondingly the Al_2O_3 particles size. However, the bending strength of the composite is still higher than that of the Ti_2AlC phase, which is 384 MPa [30], for most sintering temperature. The hardness and bending strength of the $Ti_2AlC/TiC/Al_2O_3$ in situ composite is shown in Figure 6.

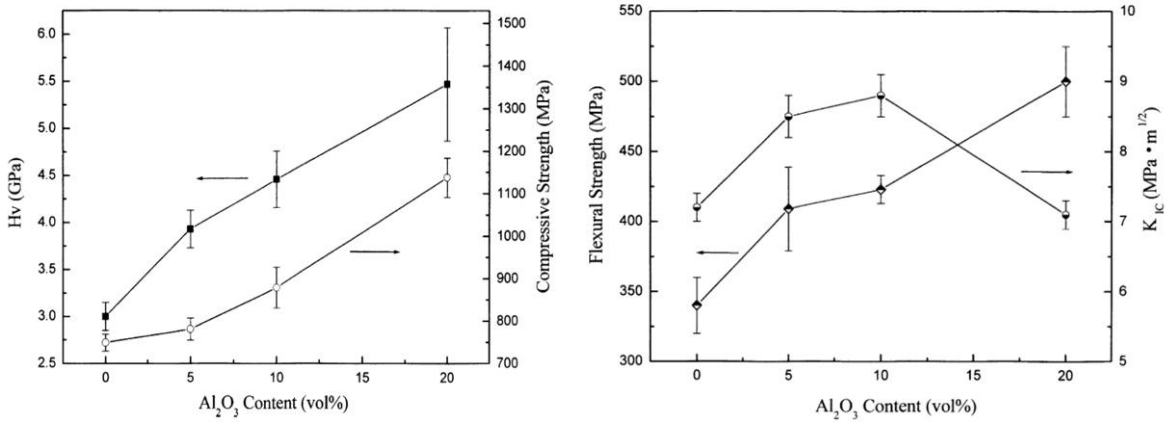

Figure 7. Vickers hardness, compressive strength, flexural strength and fracture toughness depending on the vol % of Al_2O_3 in Ti_3AlC_2/Al_2O_3 composites [31].

Chen et al. [31] fabricated Ti_3AlC_2/Al_2O_3 composites using in situ hot pressing/solid-liquid reaction process at 1500 ^oC and 1400 ^oC for 30 min, respectively, under 15 MPa in Ar, starting with the mixture of Ti (99%, 300 mesh), Al (99.5%, 300 mesh), graphite (98%, 200 mesh) and α-Al_2O_3 (99%, d=1.5um) powders. Four specimens of composites were prepared with volume fraction of Al_2O_3 from 5 to 20 vol%. In the meantime, the XRD diffraction patterns of composites showed that there was no reaction between Ti_3AlC_2 and Al_2O_3. As it can be seen in Figure 7 that summarizes results of mechanical testing from this study, the hardness, compressive

strength and flexural strength can be enhanced from 3 to 5.5 GPa, from 749 to 1138 MPa, and from 380 to 500 MPa respectively, with the increasing Al_2O_3 vol %. However, the fracture toughness was found to increase with increasing content of Al_2O_3 only up to 10 vol %.

Besides addition of reinforcing particles, solid solution strengthening has been shown to be potentially good method for strengthening Ti_2AlC. The relatively weak bonding between Al layers and Ti_6C is one of the main reasons for the low hardness and strength of Ti_2AlC. This means that the properties of Ti_2AlC can be improved by changing electronic structure and strengthening the chemical bonds. Solid solution is one of the effective methods to tailor the strength of atomic bonds.

Table 5. Calculated lattice parameters with densities for $(Ti,V)_2AlC$ solid solutions [32].

	a = b (Å)	c (Å)	Calculated Density (g / cm^3)	Measured Density (g / cm^3)
$Ti_2AlC_{0.9}$	3.0508	13.6227	4.067	4.029
$(Ti_{0.95}V_{0.05})_2AlC$	3.0486	13.6070	4.097	4.078
$(Ti_{0.9}V_{0.1})_2AlC$	3.0394	13.5808	4.139	4.110
$(Ti_{0.85}V_{0.15})_2AlC$	3.0313	13.5518	4.179	4.169
$(Ti_{0.8}V_{0.2})_2AlC$	3.0219	13.5293	4.222	4.212

In one of the first systematic studies on solid solution strengthening in Ti_2AlC, some of Ti atoms were replaced with V to form $(Ti,V)_2AlC$ [32]. The specimens were prepared by solid solution treatment to form $(Ti_xV_{1-x})_2AlC$ where X was varied from 1 to 0.8 (i.e. X=1, 0.95, 0.9, 0.85 and 0.8), during in situ hot pressing. Ti, V, Al, and graphite powders were mixed in stoichiometric ratios by ball milling for 12 hrs and cold pressed at 10 MPa and then sintered up to 1450 °C for 60 min under the pressure of 20 MPa. Table 5. shows calculated lattice parameters with densities for $(Ti,V)_2AlC$ solid solutions.

The lattice constant 'a' and 'b' decrease from 3.0508 Å to 3.0219 Å while the lattice constant 'c' decreased more significantly from 13.6227 Å to 13.5293 Å. With the decrease of the lattice constants, the calculated and measured densities then increased resulting in a fully dense material. The decrease of lattice parameters with addition of V was the first indirect evidence of stronger atomic bonds in solid solutions when compared to the pure Ti_2AlC. The Vickers hardness tested at a load of 10 N with a dwelling time of 15 s showed almost linear increase with increasing V content, as shown in Figure 8. The Vickers hardness increases from 3.5 GPa for pure Ti_2AlC to 4.5 GPa for $(Ti_{0.8}V_{0.2})_{o.2}AlC$. In the case of shear and flexural strength, a significant increase of strength was observed with increase of V content up to 10 at%. Above 10 at%, V content, the strength increases only slightly with further increase if V content as it is shown in Figure 9. Even though there is a significant decrease in compressive strength above 800 °C, the compressive strength of $(Ti_{0.85}V_{0.15})_2$ is higher than that of Ti_2AlC along the temperature range, Figure 10.

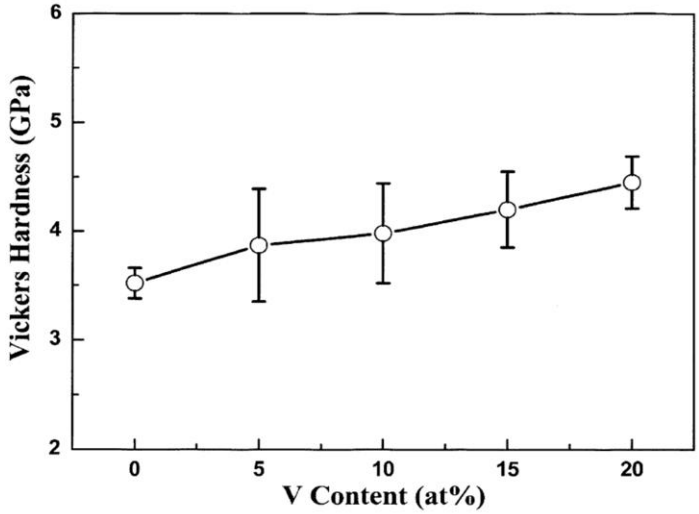

Figure 8. Vickers hardness versus V content at room temperature [32].

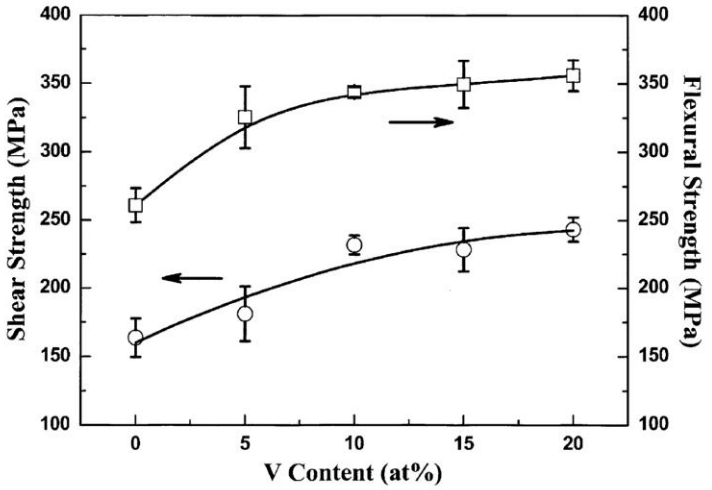

Figure 9. Flexural strengths and shear strengths as a function of V content [32].

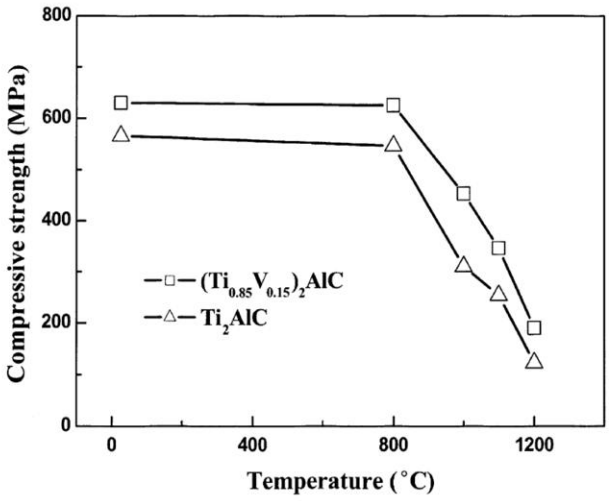

Figure 10. Temperature dependence of compressive strengths [32].

1.4 Ti_2AlC Phase Reinforced with Ceramic Fibers

Through many experimental results, it has been shown that oxide ceramic, such as alumina, Al_2O_3, is a good choice as a reinforcement phase, predominantly because it does not chemically react with Ti_2AlC. This makes it reasonable to expect that alumina fibers can be also excellent constituents to further reinforce Ti_2AlC and increase its fracture toughness, stiffens, strength and creep resistance. Usually, these oxide ceramic fibers are chemical resistant and have good strength and durability at high temperature [33].

To the best of our knowledge, there are only two studies on ceramic fiber reinforced Ti_2AlC in the open literature. In the first study, Spencer et al. [34] showed that Ti_2AlC cannot be reinforced with SiC because SiC reacts with Ti_2AlC powder

resulting in the formation of $Ti_3(Al_{1-x}Si_x)C_2$,TiC and $Al_{1+x}Ti_{1-x}$, where x ranges from 0 to 1.

In another study, Spancer et al. [35] showed that Ti_2AlC can be in principle reinforced with Al_2O_3 fibers. The samples in this study were prepared by dry mixing of alumina fibers and with Ti_2AlC powders, and subsequent densification by HPing or HIPing. As shown in this study, the sintering temperature has to be kept below 1500 ^oC to prevent decomposition of Ti_2AlC and extensive sintering of alumina fibers to each other. It has been shown that samples prepared at 1300 °C were fully dense, with no apparent reaction between fiber and matrix. In samples HPed to 1500°C, even pure Ti_2AlC powders dissociated to Ti_3AlC_2 according to: 2 Ti_2AlC = Ti_3AlC_2 + $TiAl_x$ (liq.) + (1 - x) Al (liquid/vapor), with $x < 1$. More severe Al loss results in the formation of TiC_y. The presence of the Al_2O_3 fibers delayed densification enough to allow most of the Al and Ti to escape resulting in the more intensive dissociation of the Ti_2AlC. In addition, dry mixing of fiber-powder mixture used in this study, resulted in pure dispersion of alumina fibers in the fabricated composites and their agglomeration. This, in turn resulted in extensive sintering of the alumina fibers to each other during densification of the composites.

In order to exploit the benefits of fiber reinforcement to the full extent, alumina fiber reinforced Ti_2AlC have to be fabricated with finely dispersed individual alumina fibers fully surrounded with Ti_2AlC matrix. In this thesis work, we have used aqueous dispersions of fibers and powders, in combination with slip casting to obtain green bodies of composites with finely dispersed reinforcing fibers in the Ti_2AlC matrix. The

effect of the fiber reinforcement on the elastic moduli, hardness, and fracture toughness of composites was also studied in this work.

2. MATERIALS AND EXPERIMENTAL PROCEDURE

2.1 Materials

A Ti_2AlC powder [3-ONE-2, Voorhees, NJ] was used in this study for all samples. The powders were sieved to get powders with the different distributions of particle sizes.

To reinforce the Ti_2AlC composite, two different alumina fibers were used. One is Nextel^{TM} 720 [3M, St. Paul, MN, composition : 85% Al_2O_3 and 15% SiO_3] with diameter of 10 μm and average length of 32 mm. The other one is grinded ALBF1 [Zircar Ceramic, Florida, NY, composition : 97% Al_2O_3 and 3% SiO_3] which had 3 μm diameter and average length of 150 μm. Figure 11 and 12 display two types of ceramic oxide fibers.

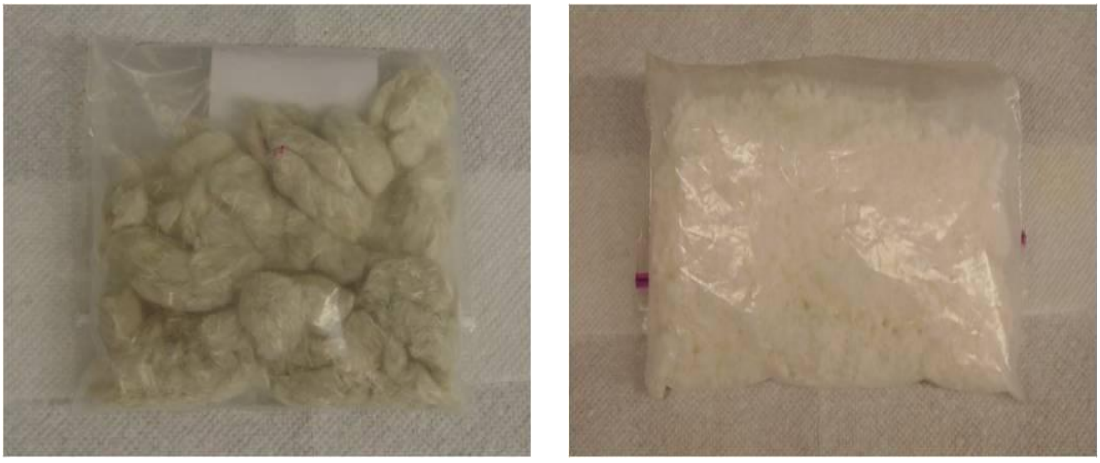

(a) (b)

Figure 11. Alumina fibers (a) Nextel^{TM} 720 (b) ALBF1.

In case of Nextel^{TM} 720, it was hard to mix the fibers with Ti_2AlC powder because fibers easily entangled by each other regardless of the mixing methods due to their large length. To prevent the entanglement, Nextel^{TM} 720 fibers were grinded by using mortar until the average length of the fiber became about 150 um which is the same average length of the ALBF1. The grinded Nextel^{TM} 720 and optical microscope images of the two ceramic oxide fibers are shown in Figure 12.

(a)

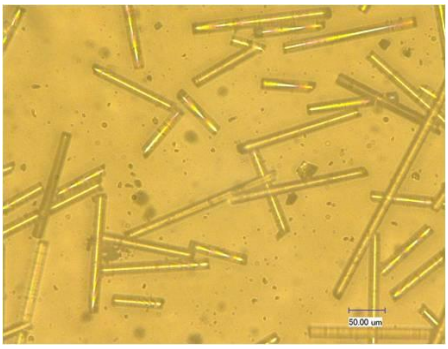

(b) (c)

Figure 12. Alumina fibers after being grinded (a) Grinded Nextel^{TM} 720. Optical micrographs of (b) Nextel^{TM} 720 (c) ALBF1.

Among oxide ceramic fibers, alumina-silicate fiber Nextel^{TM} 720, which was developed by 3M corporation, is one of the favorable oxide ceramic fiber for reinforcing high-temperature composites because of its excellent strength and high creep resistance. Nextel^{TM} 720 is composed of 85 % AlO_3 – 15 % SiO_2 by weight and designed for load bearing application in other materials. In addition, Nextel^{TM} 720 is high creep resistant. The typical properties of Nextel^{TM} 720 are shown in Table 6.

Table 6. Typical properties of Nextel^{TM} 720 [36].

Property	Units	Nextel^{TM} 720
Chemical Composition	wt %	85 Al_2O_3, 15 SiO_2
Melting Point	^{o}C	1800
Filament Diameter	um	10 ~12
Crystal Size	nm	< 500
Crystal Phase		a-Al_2O_3 + Mullite
Density	g/cc	3.4
Filament Tensile Strength (25.4 mm gauge)	MPa	2100
Thermal Expansion (100 ~ 1100 ^{o}C)	ppm/ ^{o}C)	6.0

Wilson et al. [37] measured the tensile strength and creep properties of Nextel^{TM} 720 for the first time. The single filament strength of Nextel^{TM} 720, which has 25 mm gauge length, was found to be 2100 MPa at room temperature and 1450 MPa at 1200 ^{o}C. In Figure 13, the tensile strength of Nextel^{TM} 720 at different temperatures is compared to the Nextel^{TM} 610 – a pure alumna fiber. As it can be seen in Figure 13, Nextel 720 has much better strength at temperatures above 900 ^{o}C than Nextel 610. Wilson et al. [37]

also demonstrated a good creep resistance of Nextel. Creep of Nextel 720 was found to be negative below 138 MPa at 1093 ^{o}C.

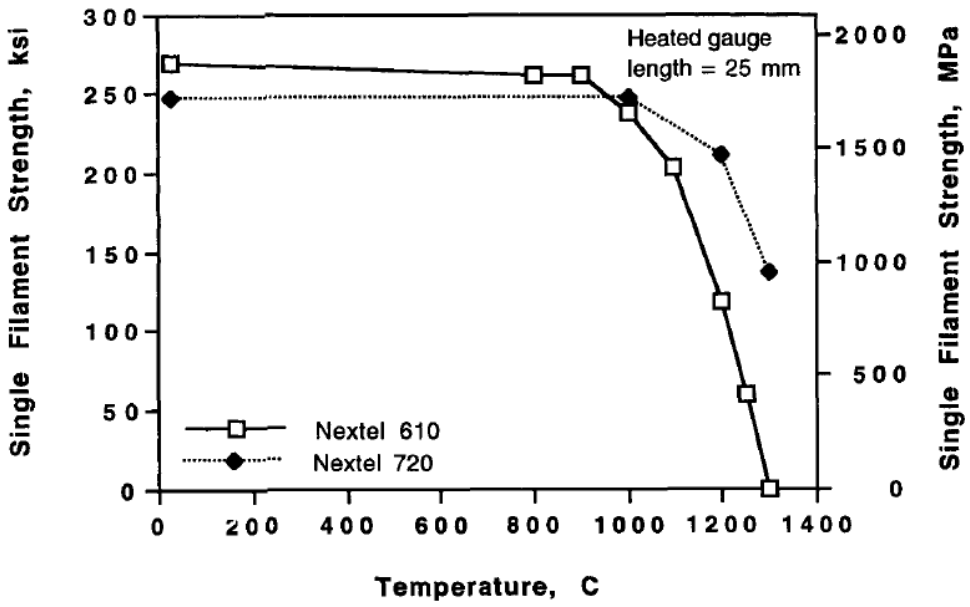

Figure 13. Tensile strength of Nextel^{TM} 610 and Nextel^{TM} 720 [37].

Since Wilson et al. published the first results on mechanical properties of Nextel^{TM} 720, several other studies have examined the mechanical properties of Nextel^{TM} 720. Deleglise et al. [38] measured the room temperature tensile properties of single filament of Nextel^{TM} 720 at different gauge lengths, between 5 and 250 mm. The tensile strength and failure strain increased as the gauge length decreased and the Young's modulus almost stayed constant. The results of this work are summarized in Table 7.

Table 7. Room temperature tensile properties of single filament of Nextel^{TM} 720 [38].

Gauge length (mm)	Tensile strength (GPa)	Failure strain (%)	Young modulus (GPa)
250	1.30 ± 0.29	0.52 ± 0.13	249 ± 14
100	1.55 ± 0.27	0.62 ± 0.10	250 ± 10
50	1.62 ± 0.33	0.67 ± 0.12	255 ± 11
25	1.68 ± 0.39	0.66 ± 0.16	252 ± 09
10	1.90 ± 0.38	0.81 ± 0.18	256 ± 27
5	1.92 ± 0.48	0.95 ± 0.24	243 ± 09

In addition to Nextel^{TM} 720, ALBF1 alumna fibers were used in this study for reinforcing Ti_2AlC. ALBF1 fibers are mostly used for thermal insulation. Their properties are briefly summarized in Table 8.

Table 8. Typical properties of ALBF1.

Property	Units	ALBF1
Chemical Composition	wt %	97 Al_2O_3, 3 SiO_2
Melting Point	^oC	2038
Filament Diameter	Um	3
Color	-	White
Shrinkage	%	2 (1 hr at 1538 ^oC) 4 (1 hr at 1650 ^oC)
Density	g/cc	3.4
Heat Capacity	J/g-^oC	1.05
Thermal Conductivity	W/m-k	1.05

2.2 Synthesis

Different methods used in this work to process pure and Al_2O_3 fiber reinforced Ti_2AlC are summarized in Figure 14.

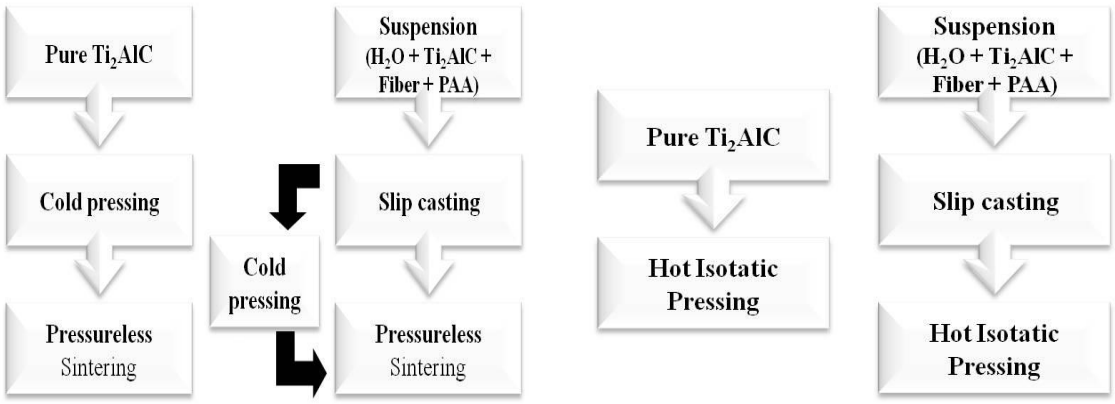

(a) (b)

Figure 14. Synthesis process pure Ti_2AlC and Ti_2AlC composite.

Mixing of the powder and fiber was carried out in two ways: i) dry mixing in glass bottle placed on a ball mill; and ii) dispersion in deionized water and mixing with a magnetic stirrer. For the first mixing method, two glass bottles were filled with Ti_2AlC powder and alumina fibers and ball mill for 4 hrs. For the second mixing method, test tubes were filled with deionized water, dispersant, and different amounts of alumina fibers. The test tubes were then shaken until beginning of entanglement of the fiber was

observed. After that, the Ti_2AlC powder was added to the fibers dispersed in aqueous solutions.

The suspensions were prepared by adding Poly-Acrylic-Acid (PAA) to deionized water. Sun et al. [39] showed that the addition of 2 dwb% PAA provided a good dispersion of Ti_2AlC powders in the slurry with an excellent fluidity. The pH of the suspension was adjusted to the desired value by adding hydrochloric acid (HCl) or sodium hydroxide (NaOH). Different amounts of alumina fibers were dispersed first in the PAA aqueous solutions. Finally, the suspension was prepared by adding Ti_2AlC powders. The process of suspension preparation is shown in Figure 15. The suspension was stirred continuously at a moderate speed before slip casting to maintain the dispersion status of ceramic oxide fibers and Ti_2AlC powders.

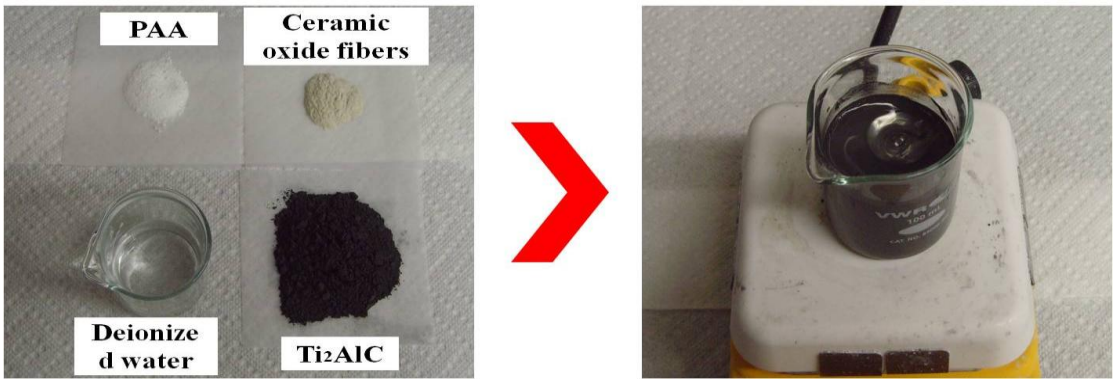

Figure 15. Process of suspension preparation.

To determine optimum amount of dispersant and pH of the slurry, a sedimentation tests were carried out for both, fiber and Ti_2AlC powder dispersions. For the sedimentation measurement, suspension was prepared by dissolving different

amounts of PAA dispersant in deionized water. A small amount, usually 1 vol%, of Ti_2AlC powder or alumina fibers were added in PAA aqueous solutions. 11 test tubes were filled with 2.5 ml of the suspension of fibers or powders in PAA aqueous solutions.

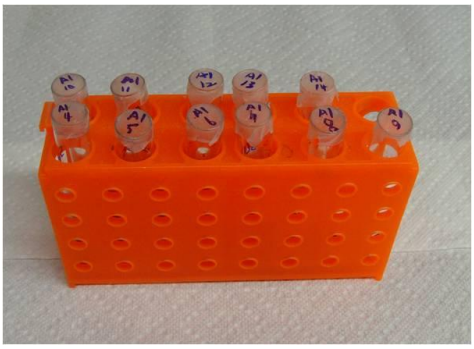

(a)

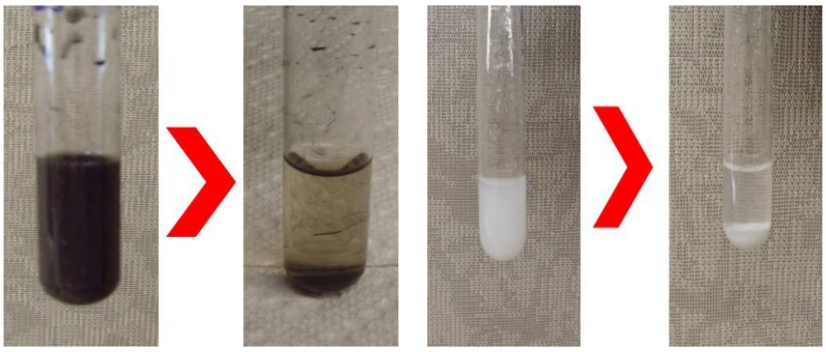

(b) (c)

Figure 16. Sedimentation measurement (a) test tubes (b) Ti_2AlC powder (c) alumina fiber.

The pH of the slurry in each test tube was adjusted from pH 4 to 14 by hydrochloric acid (HCl) or sodium hydroxide (NaOH). The test tubes were covered with Parafilm [Pechiney Plastic Packaging Company, Chicago, IL] to avoid the evaporation of water.

Then each test tube was shaken until Ti_2AlC powder and/or fibers were dispersed evenly in the solvent. The sedimentation time was evaluated until significant flocculation was observed. The set up for sedimentation measurement are shown in Figure 16 together with the typical photographs of the dispersion before and after sedimentation tests. Once optimum conditions for colloidal dispersion of powders and fibers were determined from sedimentation tests, the slurries containing colloidal suspensions of fibers and powders were slip cast into molds, to process green bodies of composites.

Colloidal processing employed in this work to fabricate alumina fiber reinforced Ti_2AlC composites has been used to produce ceramic materials for several centuries. A colloid consists of the micro-particles that are dispersed evenly throughout the solvent. The colloidal processing of ceramics has many advantages compared with the dry powder processing method. The colloidal processing method is good for minimizing strength-degrading defects, forming complex shapes, tailoring the microstructure, making large size products, and most importantly obtain homogenous distribution of different phases in multi-phase systems [40]. During the colloidal processing, it is important to make the suspension to be dispersive and stable for good quality of the products. Among many types of suspension methods, aqueous suspension is favored because it is allows a fast removal of the solvent before sedimentation and segregation of the suspension. In addition, it is a safe, economical, and environmentally friendly technique.

Slip casting is one of the colloidal processing methods. A slip, i.e. suspension, is prepared by mixing water and non-plastic materials. Then, a suspension is poured into a

mold to absorb water from a suspension. As the cast piece dries, it shrinks simultaneously. Once the suspension is completely dry, the mold is disassembled and the cast piece is removed from the mold. Among mold materials, plaster of Paris is commonly used because it is economical and easy to use for fabricating complicated shapes. After consolidation in room temperature, the cast piece is usually additionally dried in the oven at certain temperature and then sintered in a high temperature furnace. Sometimes, argon gas is fluxed into the furnace to avoid possible oxidation. The stages of the slip casting are shown in Figure 17.

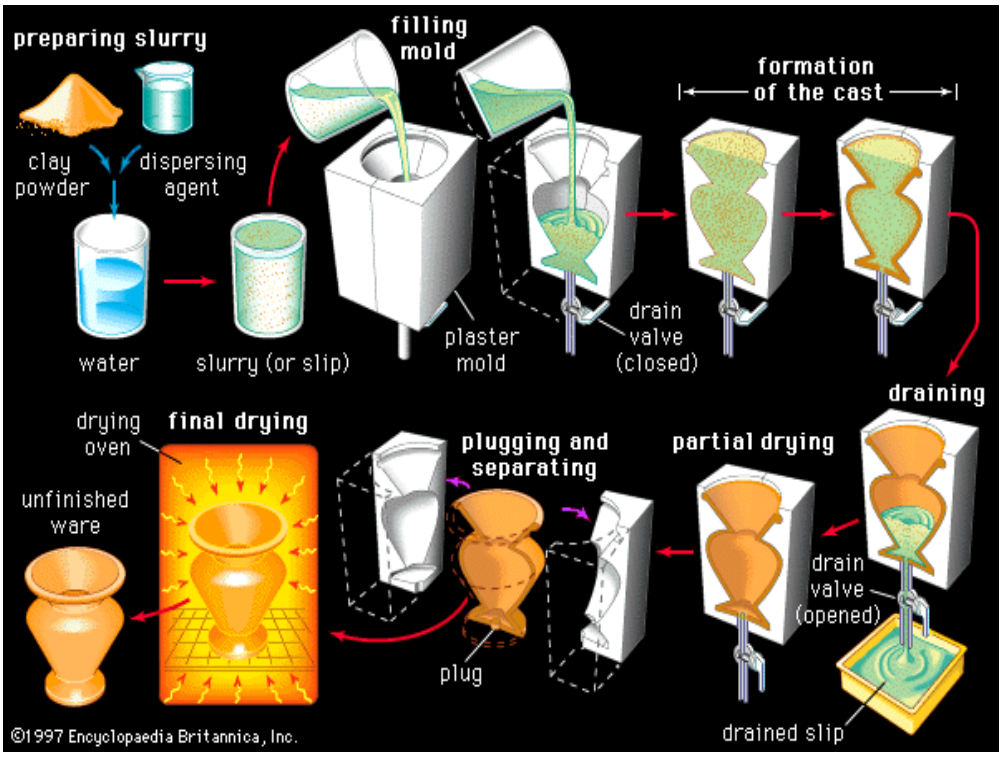

Figure 17. Stages of slip casting.

For the Ti_2AlC composite reinforced by the alumina fibers, the mold was prepared by using plaster [DAP Inc, Baltimore, MD]. One cylindrical insert with preferred size was placed in the middle of the mold to make a mold cavity. For the samples sintered by Hot Isostatic Pressing, HIPing, the cylindrical insert had the same size as the glass beaker so that green body after the slip casting can fit in 30 ml glass beaker [VWR, Arlington Heights, IL] completely without breaking the green body.

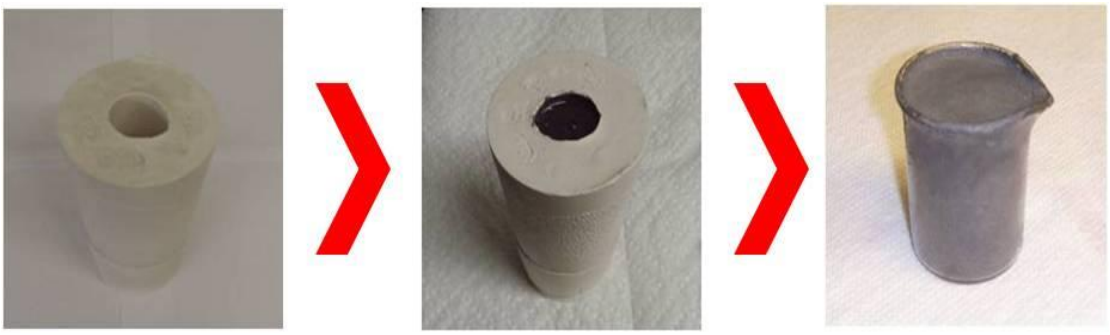

(a) (b) (c)

Figure 18. Process of the slip casting (a) mold (b) mold with suspension (c) beaker for HIPing.

Once the mold was prepared, it was dried out in the oven until slip casting. This is done because the dried plaster mold can absorb water from the suspension efficiently and consolidate the suspension rapidly. This method also helps the green body to maintain good susspension of Ti_2AlC powder and ceramic oxide fibers by reducing the duration of liquid state in the mold. The suspension was then poured into the dry mold. As the water of the suspension was absorbed by the mold, the green body became consolidated.

After consolidation for 30 min, the green body removed from the mold and dried at 80 ℃ for 24 hrs. For the sintering by HIPing, the slip casting product was placed into a glass beaker for HIPing. The process of the slip casting is shown in Figure 18.

It is worth noting here that some of the initial suspensions were prepared with adding additionally an organic binder such as Butvar, PVA and Cellulose to the colloidal suspension of ceramic powders and fibers. However, since green bodies processed without binder had enough strength for handling them during additional cold pressing and sintering, all samples used in this study were prepared without binder. Additional reason for preparing suspensions without organic binders is possible reaction of the organic binder with MAX phases and formation of TiC, as it was previously reported in the literature [41].

Green bodies (dried suspensions) of composites were further densified by cold pressing and pressurless sintering, PSing. To process pure Ti_2SiC, the powders were only cold pressed and subsequently presureless sintered, as illustrated in Figure 14. The processing conditions for the various pressureless sintered samples are shown in Table 9. Note that some of the pressures sintered samples were previously slip cast, some were only cold pressed, and some were slip cast and additionally cold pressed.

Table 9. The various pressureless sintering samples.

Sample	Material	Green body processing	Ti_2AlC Powder size (μm)	Cold pressing pressure (MPa)	Presureless sintering
PS1	Ti_2AlC	Coldpressing	-32	800	4 hours at 1300 °C
PS2	Ti_2AlC	Coldpressing	-90	800	4 hours at 1300 °C
PS3	Ti_2AlC	Coldpressing	-90 (90wt%) -20 (10wt%)	800	4 hours at 1300 °C
PS4	Ti_2AlC	Coldpressing	-32 (90wt%) -20 (10wt)	800	4 hours at 1300 °C
PS5	Ti_2AlC	Coldpressing	-20	800	4 hours at 1400 °C
PS6	Ti_2AlC	Slipcasting with 2dwb%PAA, pH=4	-20	-	4 hours at 1200 °C
PS7	Ti_2AlC	Slip casting with 2dwb%PAA, pH=4 and Coldpressing	-20	400	4 hours at 1300 °C
PS8	Ti_2AlC+ 10vol% Nextel 720	Slipcasting with 2dwb% PAA, pH=4	-20	-	4 hours at 1200 °C
PS9	Ti_2AlC+ 10vol% Nextel 720	Slip casting with 2dwb%PAA, pH=4 and Coldpressing	-20	800	4 hours at 1200 °C
PS10	Ti_2AlC+ 10vol% Nextel 720	Slip casting with 2dwb%PAA, pH=4 and Coldpressing	-20	800	4 hours at 1400 °C
PS11	Ti_2AlC+ 10vol% Nextel 720	Slip casting with 2dwb%PAA, pH=4 and Coldpressing	-20	1900	4 hours at 1400 °C
PS12	Ti_2AlC+ 4vol% ALBF1	Slip casting with 2dwb%PAA, pH=4 and Coldpressing	-90	800	4 hours at 1400 °C

Samples PS1-PS5 were processed by cold pressing pure Ti_2AlC powders of different particle sizes and pressureless sintering at different conditions. Samples PS6 and PS7 , although pure Ti_2AlC, were processed by slip casting and further densified by cold pressing and pressureless sintering. The sample PS8 was made by slip casting,

while samples from PS9 to PS12 were made through the slip casting and additional cold pressing of Ti_2AlC powder and Al_2O_3 fiber mixtures. First, the green bodies were made by slip casting and then loaded in a steel die and pressed to loads corresponding to 400 ~ 1900 MPa for 5 min. Then these were sintered in a high temperature furnace with fluxing argon heating at various temperatures for 4 hrs.

After the slip casting and/or cold pressing was completed, the green body was sintered in a sealed high temperature furnace with fluxing argon heating at various temperatures for 4 hrs. The equipments for pressureless sintering and cold pressing are shown in Figure 19.

(a) (b)

Figure 19. Equipment for pressureless sintering (a) high temperature furnace [Model : GSL-1600, MTI Co, Richmond, CA] (b) steel die for cold pressing.

In addition to presureless sintering, three different samples were densified by HIPing, Figure 14b. The HIPing is widely used in research and industry for production of various materials and ceramics. The HIP equipment mainly consists of HIP pressure

chamber with furnace, PLC (Programmable Logic Controller), and PC, as shown in Figure 20. The major advantage of HIP when compared to the pressureless sintering is that the HIPed materials have very high density compared to the other methods due to application of high isotropic pressure during sintering at temperature well below the melting point of the material. In general, as the heat is being provided during HIPing, the isotropic pressure is being applied to the material simultaneously by pressurized inert gas. The common gases used in pressurizing the materials are mainly nitrogen and argon, but the usage of other gases like oxygen is also possible.

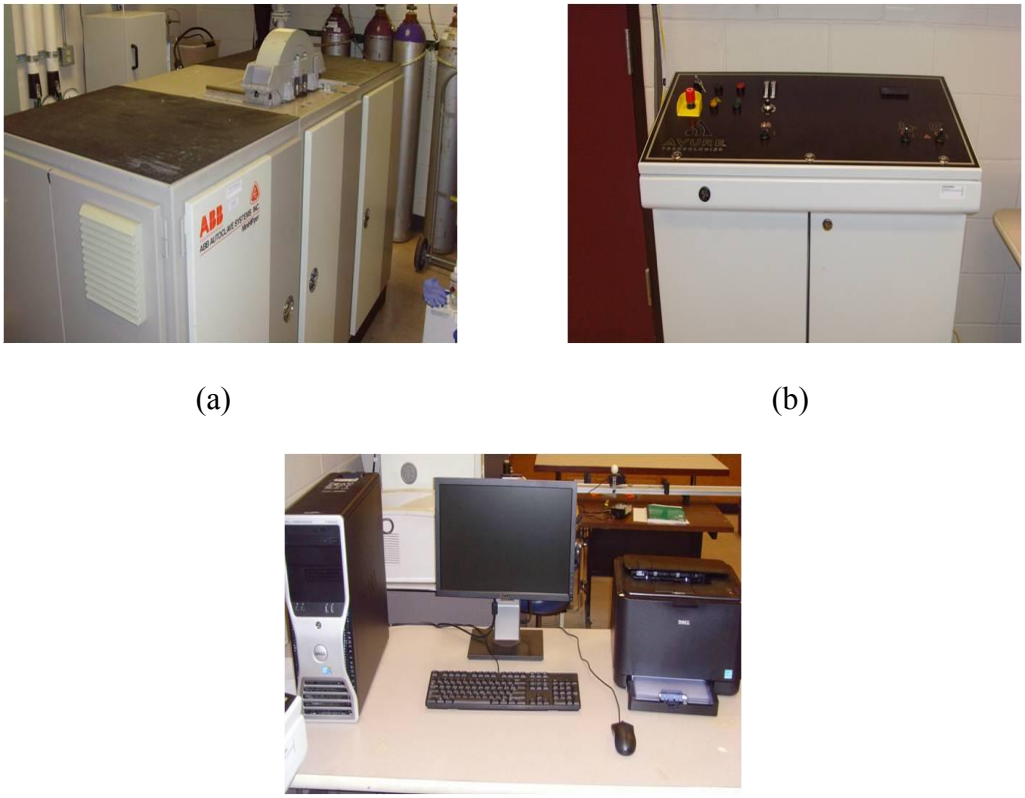

(a) (b)

(c)

Figure 20. HIP components (a) HIP (b) PLC (c) PC.

Three different green bodies of Ti_2AlC composite were prepared for HIPing. One sample was prepared by HIPing pure Ti_2AlC [-450 mesh] powders. The two other samples, namely Ti_2AlC composites with alumina fibers (Grinded Nextel^{TM} 720 and ALBF1 fibers.), were prepared by slip casting since alumina fibers had to be dispersed in the liquid before mixing with Ti_2AlC powder, and subsequent HIPing. For slip casting, 2 dwb% Poly-Acrylic-Acid (PAA) [SIGMA-ALDRICH, St. Louice, MO] and deionized water were used as a dispersant and dispersing medium respectively. The synthesis process for HIPed samples is schematically shown in Figure 20, while processing conditions are listed in Table 10.

Table 10. The samples prepared by Hot Isotatic Pressing.

Sample	Material	Process	Particle Ssize (um)	HIPing Pressure (MPa)	HIPing time and Temperature
H1	Ti_2AlC	-	-32	100	4 hours at 1300 °C
H2	Ti_2AlC+ 5vol% 720	Slip casting with 2dwb%PAA, and pH=4	-32	100	4 hours at 1300 °C
H3	Ti_2AlC+ 5vol% ALBF1	Slip casting with 2dwb%PAA, and pH=4	-32	100	4 hours at 1300 °C

HIPing of all samples in this study was carried on in graphite crucible. The inside of the graphite crucible was covered with graphite foil to make it easy to take the sample out after HIPing. The glass beaker including green body was placed in graphite crucible and embedded in a bed of crushed borosilicate glass [Fisher Scientific Inc, Pittsburgh, PA]. The HIP [Avure Technologies, Inc, Kent, WA] was sealed and evacuated. The temperature was increased up to 900 ℃ at 4 ℃/min. Then the temperature was held for 60 min while pressurizing with argon up to 14500 psi. After pressurizing, the temperature ramped to 1300 ℃ at 10 ℃/ min and held at this temperature for 4 hrs. Then the furnace was cooled down slowly. The programming for temperature and pressure is showed in Table 11 and Figure 21.

Table 11. The programming for HIPing.

Segment	Temperature (℃)	Pressure (psi)	Segment Time (min)
1	0	0	0
2	900	0	225
3	900	14500	60
4	1300	14500	40
5	1300	14500	240
6	900	0	40
7	400	0	50
8	50	0	Free cooling

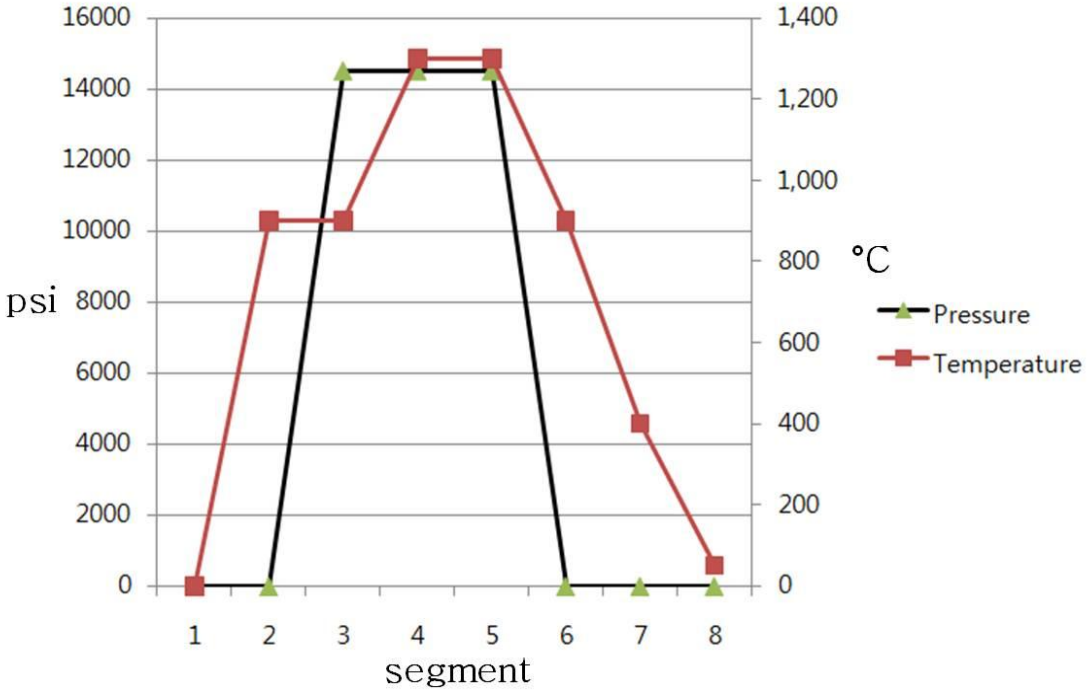

Figure 21. The programming parameters for HIPing.

After the HIPing, the sample was covered with melting borosilicate glass. The glass surrounding the sample was removed by using a bench grinder. The HIPing process is illustrated in Fig 22.

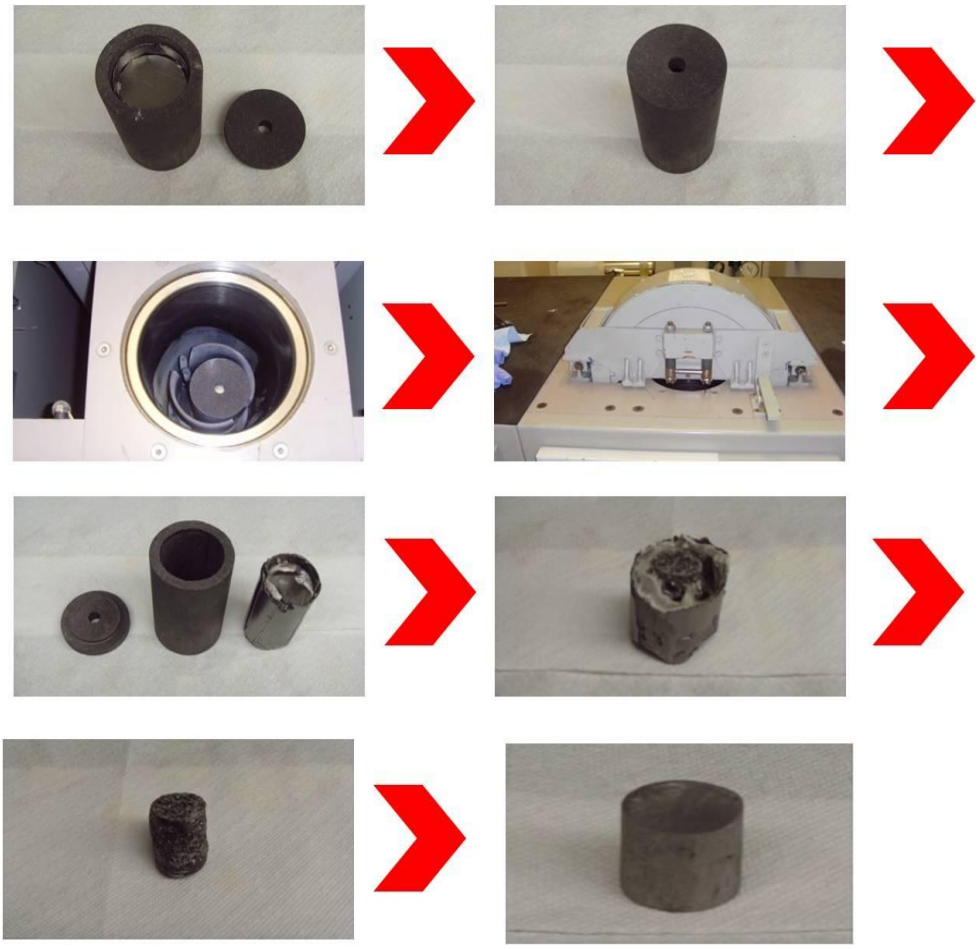

Figure 22. HIPing process.

2.3 Structural Characterization of Composites

The density of all samples was measured according to ASTM Standard C20-00 using alcohol immersion method. First, the dry weight of the sample was measured before it was immersed in alcohol in vacuum for 5 min. After 30 min, the temperature of alcohol was checked and the corresponding density of alcohol was calculated. Then the suspended weight of the sample was measured. Finally, the weight of the sample was

measured after removing from alcohol and covered with a tissue paper for 1 min to remove residue of alcohol on the surface. Then open and closed porosity and bulk density was calculated using measured values as described in ASTM Standard C200.

The structure of HIPed and pressureless sintered samples were examined by X-ray diffraction (XRD) [Model D8 Advance, Bruker AXS, Madison, WI]. Scans were carried out with CuKα radiation at a scanning rate of 1.2 deg/min, using steps of 0.02 deg. For microstructural and elemental analyses, samples were studied by a Scanning Electron Microscopy, SEM, [Quanta 600 FE-SEM, FEI Co, Hillsboro, OR] equipped with Energy Dispersive Spectroscope (EDS). Samples were prepared by mounting and polishing them up to 1 um diamond suspension. The XRD and SEM used in this study are shown in Figure 23.

(a) (b)

Figure 23. Microstructural and elemental analyses equipment (a) X-ray diffraction (XRD) (b) scanning electron microscopy (SEM).

2.4. Mechanical Characterization

Almost fully dense pure Ti_2AlC and alumina fiber reinforced Ti_2AlC composites processed by HIPing (samples H1, H2 and H3) were characterized to determine their room temperature Vickers hardness, elastic moduli and fracture toughness.

Vickers hardness of the samples were measured by Microhardness Tester [model : LM 300AT, LECO, Michigan, USA] at room temperature. Load was applied to the indenter and held for 13 seconds. Load of 300 g was used for testing in this study. Then the indentation diagonals of the sample were measured to calculate the Vickers hardness (HV) using following equation.

$$HV = 1.854 \left(\frac{P}{d^2} \right) \quad (2.1)$$

P is the applied load and d is the average length of the two diagonals of the indentation.

Figure 24. Microhardness tester.

Room temperature elastic moduli were determined by Resonant Ultrasound Spectrosocpy [Quasar International, NM] at room temperature. The sample was put on three piezoelectric transducers. One of the transducers produces excitation signal at sweeping frequency. The other two transducers are used to measure resonance response of the exited sample. The resonant spectra are used to determine elastic constant by using multidimensional software RuSpec [Quasar International, NM].

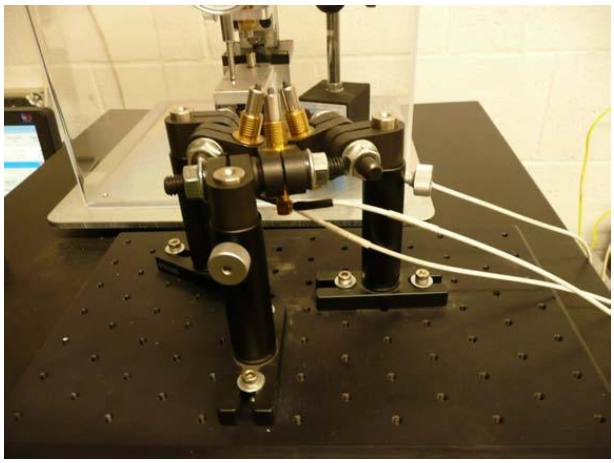

Figure 25. RUS at room temperature.

The fracture toughness (K_{1C}) provides basic information about the transverse crack resistance. The double torsion (DT) tests were carried out on the HIPed Ti_2AlC composites to determine the K_{IC} of the samples. The concept of the DT was introduced by Outwater and Gerry [42].

For the DT tests, the specimens were cut from the HIPed samples by using Electrical Discharge Machining (EDM) [FX-10, Mitsubishi Co, Japan]. The dimensions are as follows: width = 20 mm; length = 30 mm; and thickness = 1 mm. An initial notch,

which is 8 mm long, was cut into one side of the specimen by using the 0.5 mm thick diamond saw to initiate the crack from the notch. This facilitates the formation of a sharp precrack at the notch tip at low load. The specimen for DT test is shown in Figure 26.

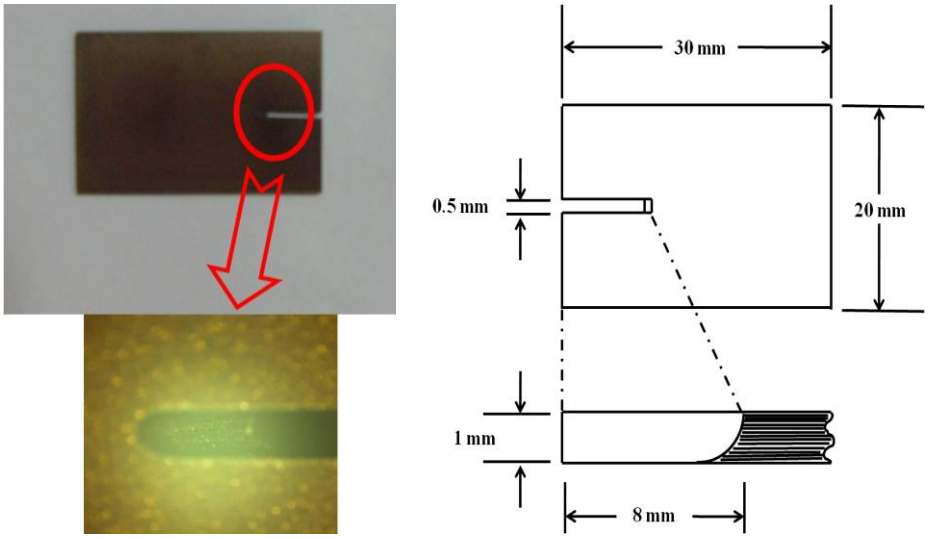

Figure 26. Specimen for DT test.

The specimen was loaded on the double torsion test fixture which has four supporting and two loading points to propagate the crack axially along the specimen. Once the specimen and the test fixture are aligned, they were located on the bottom plate of the Instron [model : 4411, PA] testing machine. All the samples were precracked by loading the sample at a rate of 0.05 in/min. Then the precacked samples were loaded at a rate of 0.5 in/min to cause fast fracture. The DT test system is shown in Figure 27. The K_{1C} of the samples were calculated by following equation:

$$K_{1C} = PS_m \left[\frac{3(1+v)}{St^4\delta} \right]^{1/2} \quad [43] \qquad (2.2)$$

where S_m (7 mm) is the moment arm, S (20 mm) is specimen width, t (10 mm) is specimen thickness, v is Poisson's ratio, P is critical load of fast fracture and δ is thickness correction factor given as [44] :

$$\delta = 1\text{-}1.26\ (t/S) + 2.4\ (t/S)\ \exp\ (-2\pi S/2t) \quad (2.3)$$

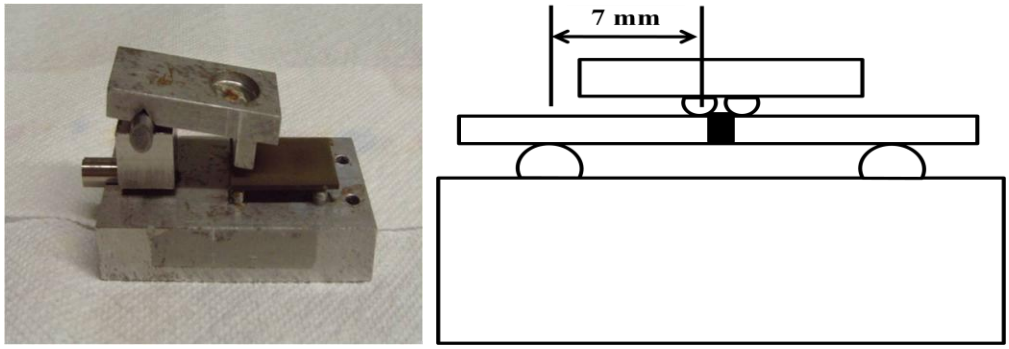

(a)

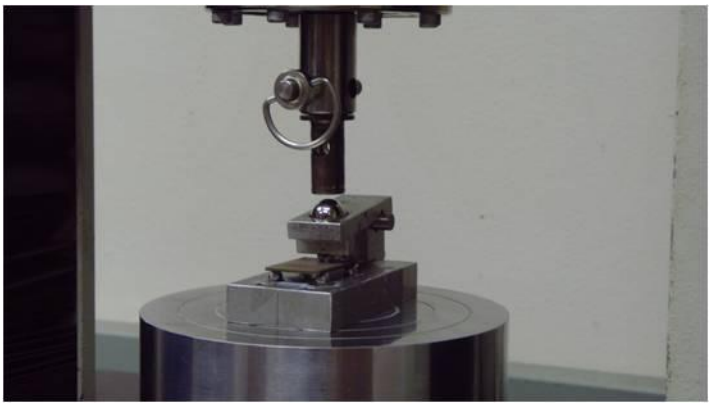

(b)

Figure 27. The double torsion test system (a) test fixture (b) loading section.

3. RESULTS AND DISCUSSION

3.1 Dispersion of the Fibers and Powders

As Spancer et al. [35] showed, Ti_2AlC can be in principle reinforced with Al_2O_3 fibers. However, dry mixing of fiber-powder mixture used in this study, resulted in poor dispersion and agglomeration of alumina fibers in the fabricated composites that consequently sinter to each other during densification of the composites. The resulting microstructure is shown in Figure 28.

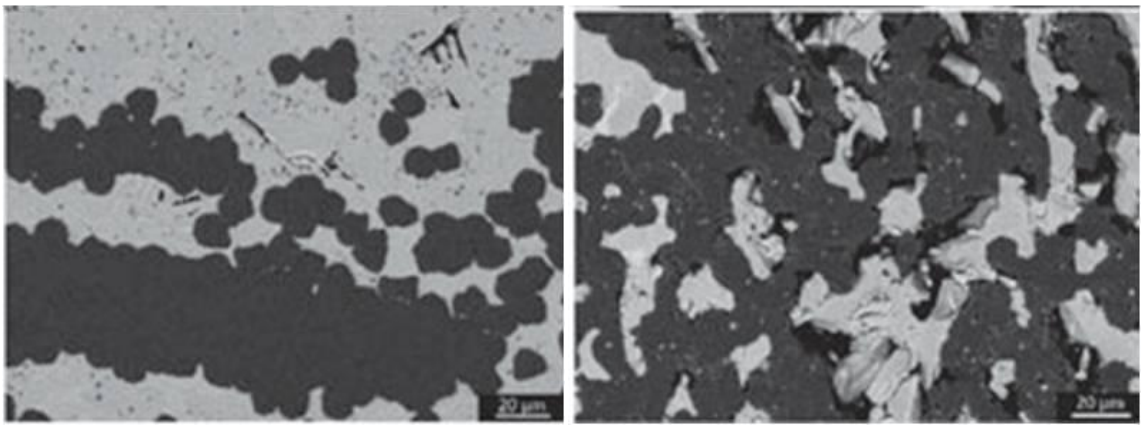

(a) (b)

Figure 28. Backscattered electron SEM images showing effect of temperature on Al_2O_3 fiber morphology. (a) 17 vol% fibers HIPed at 1300 ^oC (b) 46vol% HIPed at 1500 ^oC. The fibers agglomerated and sintered together [35].

Since high agglomeration of the fibers and their sintering to each other usually results in degradation of mechanical properties of the ceramic matrix composites, it is imperative to disperse completely the fibers in the ceramic matrix to exploit benefits of fiber reinforcement to the full extent. One way to achieve better dispersions of the fibers is to use shorter fibers, since they entangle less during dry mixing with powders.

The first method of mixing short fibers and powders in this study was dry mixing in glass bottle placed on a ball mill for 4 hrs. The result of the dry mixing was shown in Figure 29. The 5 vol% Nextel^{TM} 720 fibers were mixed with the Ti_2AlC without any significant entanglement of the fibers. In case of Nextel^{TM} 720 fiber, there was a significant increase of the volume fraction of fibers that can be dispersed in Ti_2AlC powder during dry mixing after grinding the fibers to the length of 150 μm. On the other hand, many flocculants/agglomerates were found in the ALBF1 fiber mixture. The ALBF1 fibers were entangled to each other rather than mixing with powder.

(a) (b)

Figure 29. The result of the dry mixing (a) Nextel^{TM} 720 (b) ALBF1.

The second mixing method was dispersing fibers in deionized water solution and mixed with a magnetic stirrer. The result of the second mixing method was shown in Figure 30. In case of grinded Nextel^{TM} 720, the entanglement of the fibers began to be observed in the suspension including 15 vol% fibers. In case of ALBF1, no flocculation was observed in the suspension up to 4 vol% fibers, while in the suspension with 5 vol% of fibers, a small fraction of entanglement of the fibers began to be observed although overall dispersion of the fibers was still fairly good. In the suspension with 6 vol% ALBF1 fibers, extensive entanglement of fibers was identified. This result makes it clear that 5 vol% of fibers is the appropriate amount to disperse the fibers in the suspension without significant entanglement of fibers.

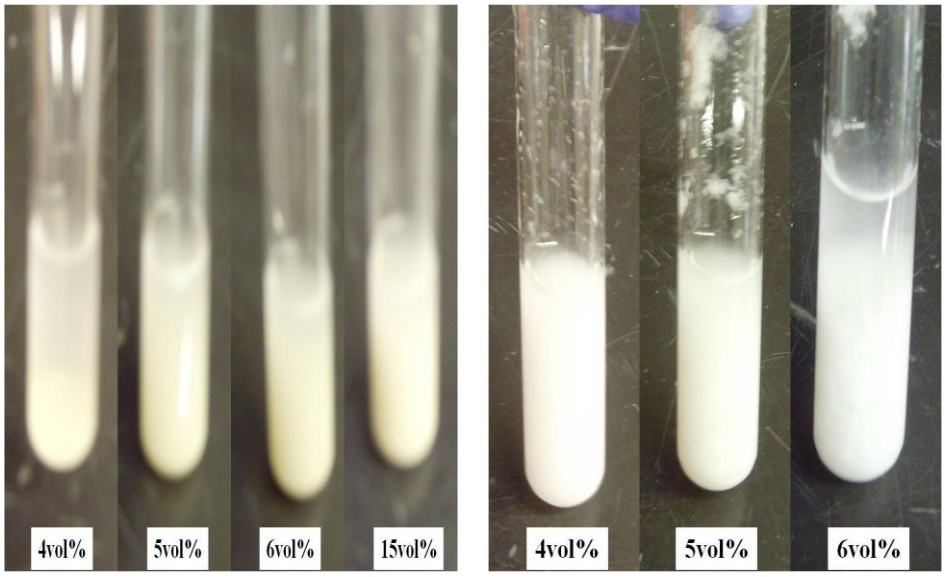

(a) (b)

Figure 30. The result of the solution mixing (a) Nextel^{TM} 720 (b) ALBF1.

From the two results of the dispersing the fibers, it was obvious that the higher amount of grinded Nextel^{TM} 720 can be dispersed in the aqueous suspensions with Ti_2AlC powders, when compared to the amount of ALBF1 fibers. This is most likely because the diameter of the Nextel^{TM} 720 (10 um) is larger than ALBF1 (3 um). Therefore, the ALBF1 was more easily bended and entangled when the fibers bumped into each other during mixing in the suspension. In addition, there were more ALBF1 fibers than Nextel^{TM} 720 in the same volume percent fibers which also increase probability of entanglement of ALBF1 fibers.

Along with the dispersing the fibers, the sedimentation time for alumina fibers was measured in solution with 2 and 5 dwb% PAA in the pH range of 4 ~ 14. The sedimentation time for ALBF1 was 3 min in pH=4 and 2 min in the pH range of 5 ~ 14. The sedimentation time for Nextel^{TM} 720 was 2 min in pH=4 and 1 min in the pH range of 5 ~ 14. The sedimentation time was same regardless of the amount of PAA (2 and 5 dwb%). Also, sedimentation time for alumina fibers was almost same even though the fibers were dispersed in the suspension with 1 vol% Ti_2AlC powder.

3.2 Stability of Ti_2AlC Suspensions

The stability of the Ti_2AlC suspensions was determined using sedimentation tests for the different amounts of PAA dispersants and different pH values of the suspension. Figure 31. shows the influence of pH and PAA on the stability of Ti_2AlC suspensions. The suspension in the 4 ~ 10 pH range showed excellent stability up to almost 315 hrs,

while there is a significant decrease of sedimentation time for the suspensions in 11 ~ 14 pH range. This result shows that the suspensions in the pH range of 4 ~ 10 are good for the slip casting because the green body, which is prepared by the slip casting, can have the uniform dispersion of the powders. The sedimentation time of suspensions with 2 dwb% PAA was slightly longer than 5 dwb%. This result reproved that the addition of 2 dwb% PAA provided MAX phase suspensions with an excellent fluidity [39].

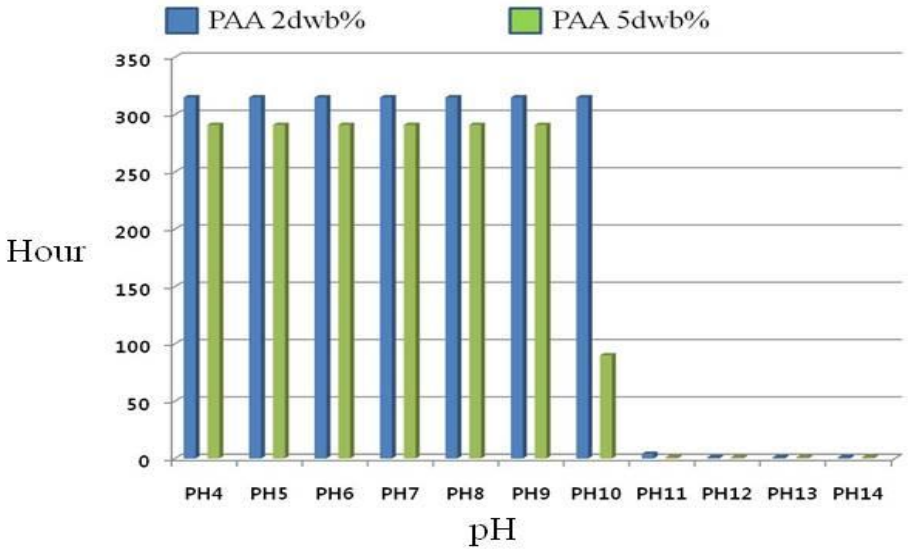

Figure 31. Sedimentation time for Ti_2AlC suspensions in the pH range of 4 ~ 14.

Based on results of the sedimentation testing of the fiber and powder suspensions, it was concluded that the suspensions with pH=4 and 2 dwb% PAA provide the most stable suspensions that would not sediment significantly during slip casting. Therefore, all mixing of the alumina fibers and Ti_2AlC was further carried on in aqueous solutions of 2 dwb% PAA with pH=4.

3.3 Pressureless Sintering

Table 12. The relative densities of the pressureless sintered pure Ti_2AlC samples.

Sample	Material	Green body processing	Ti_2AlC Powder size (μm)	Cold pressing pressure (MPa)	Presureless sintering	**Relative Density (%)**
PS1	Ti_2AlC	Coldpressing	-32	800	4 hours at 1300 ^oC	**77.24**
PS2	Ti_2AlC	Coldpressing	-90	800	4 hours at 1300 ^oC	**77.51**
PS3	Ti_2AlC	Coldpressing	-90 (90wt%) -20 (10wt%)	800	4 hours at 1300 ^oC	**77.34**
PS4	Ti_2AlC	Coldpressing	-32 (90wt%) -20 (10wt)	800	4 hours at 1300 ^oC	**76.89**
PS5	Ti_2AlC	Coldpressing	-20	800	4 hours at 1400 ^oC	**93.83**
PS6	Ti_2AlC	Slipcasting with 2dwb%PAA, pH=4	-20	-	4 hours at 1200 ^oC	**42.65**
PS7	Ti_2AlC	Slip casting with 2dwb%PAA, pH=4 and Coldpressing	-20	400	4 hours at 1300 ^oC	**74.74**

The relative densities of the pressureless sintered pure Ti_2AlC samples are shown in Table 12. This result shows that the higher sintering temperature results in the higher relative density of the sintered samples. The relative density of PS5, that was pressureless sintered at 1400 ℃, was 93.83 %. However, the pressurless sintering temperature below 1400 ℃ was not appropriate to make high density samples. The relative densities of the samples pressureless sintered at 1200 and 1300 ^oC never exceeded ~ 77.5%, which were well below relative density of the sample PS5 sintered at

1400 ℃. It is also obvious (Table 12) that cold pressing produced the samples with higher relative densities, when compared to the slip cast samples. Sample PS6 prepared by slip casting and without cold pressing had relative density of only 42.65 %., while sample PS7 that was cold pressed after slip casting reached relative density of 74.74% after pressureless sintering. This density was significantly low compared to cold pressed samples. Samples of PS1 ~ 4 were prepared with different size particles. However, there were no significant differences in the densities.

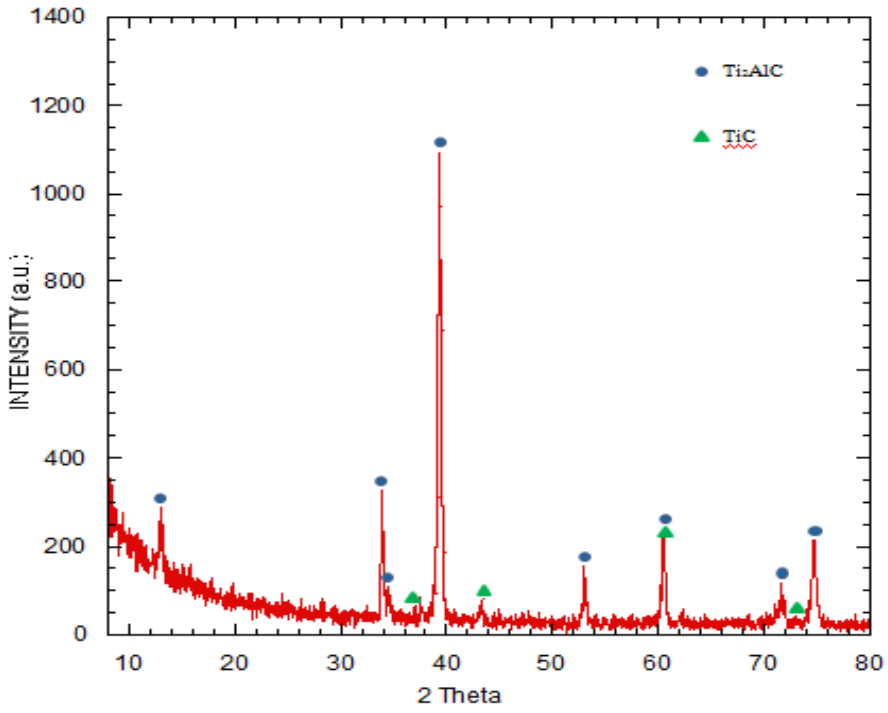

Figure 32. XRD pattern of PS5.

Figure 32 and 33 shows the XRD pattern and SEM image of PS5. Only Ti_2AlC with some TiC from initial powders was identified after sintering at temperatures as high

as 1400 ℃. Some small amount of TiC detected in the sintered samples was actually present in the initial powders. It is apparent that there was no reaction while pure Ti_2AlC powder was sintering at 1400 ℃.

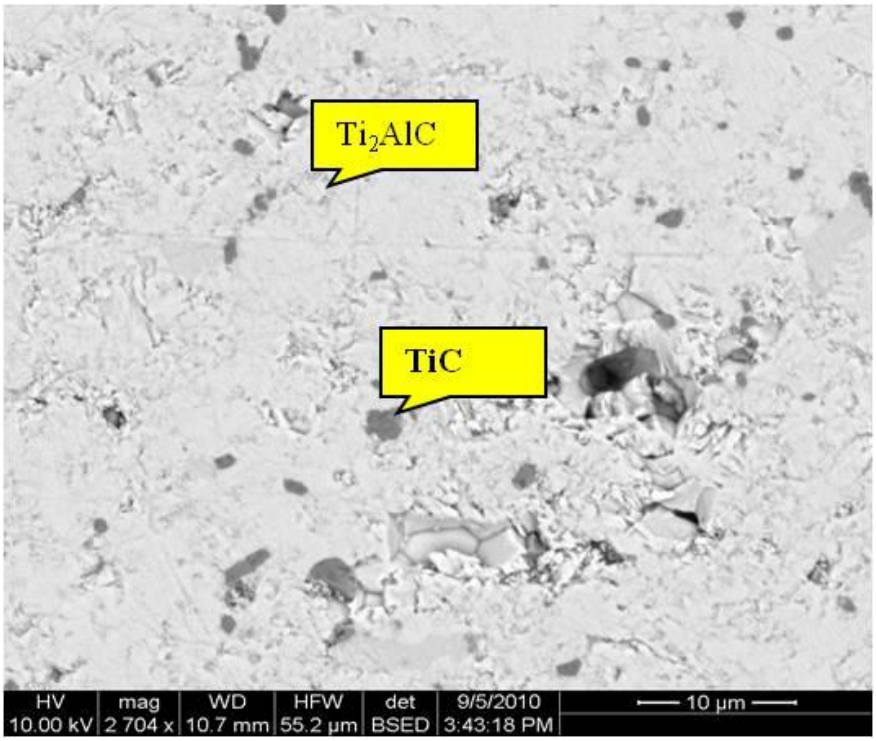

Figure 33. SEM image of PS5.

The relative densities of the pressureless sintered alumina fibers reinforced composites are shown in Table 13. This result also shows that:

- Increase in pressureless sintering temperature does not increase significantly the relative density of the composites. The relative density of PS10, which was sintered at 1400 ℃ is higher for only ~ 4% than that of PS9, which was sintered at 1200 ℃.

- Cold pressing produced the samples with high densities. PS8 was prepared by slip casting without cold pressing and had relative density of only 51.86 %, while sample PS9 that was additionally cold pressed after slip casting had relative density of 70.35% after pressurless sintering.
- The overall relative densities of the alumina fibers reinforced composite were lower compared to the pure Ti_2AlC samples, suggesting that alumina fibers hinder densification of Ti_2AlC. For example, the relative density of composite sample PS10 was only 74.85%, while the pure Ti_2AlC sample process using the same condition (PS5 in Table 12) had relative density of 93.85%. This is in good agreement with the results of previous study by Spencer et al. [35].

Table 13. The relative densities of the pressureless sintered alumina fibers reinforced composites.

Sample	Material	Green body processing	Ti_2AlC Powder size (μm)	Cold pressing pressure (MPa)	Presureless sintering	**Relative Density (%)**
PS8	Ti_2AlC+ 10vol% Nextel 720	Slipcasting with 2dwb% PAA, pH=4	-20	-	4 hours at 1200 ^oC	**51.86**
PS9	Ti_2AlC+ 10vol% Nextel 720	Slip casting with 2dwb%PAA, pH=4 and Coldpressing	-20	800	4 hours at 1200 ^oC	**70.35**
PS10	Ti_2AlC+ 10vol% Nextel 720	Slip casting with 2dwb%PAA, pH=4 and Coldpressing	-20	800	4 hours at 1400 ^oC	**74.85**
PS11	Ti_2AlC+ 10vol% Nextel 720	Slip casting with 2dwb%PAA, pH=4 and Coldpressing	-20	1900	4 hours at 1400 ^oC	**84.43**
PS12	Ti_2AlC+ 4vol% ALBF1	Slip casting with 2dwb%PAA, pH=4 and Coldpressing	-90	800	4 hours at 1400 ^oC	**83.16**

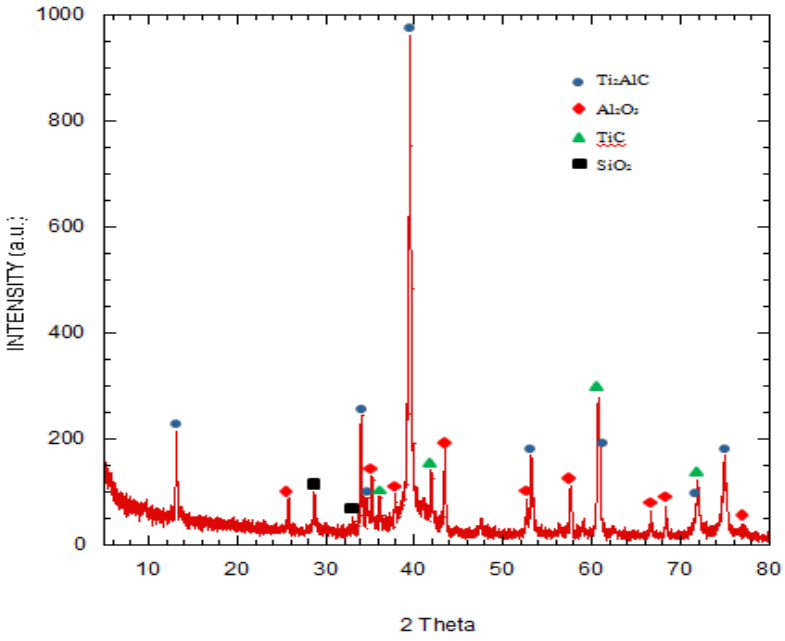

(a)

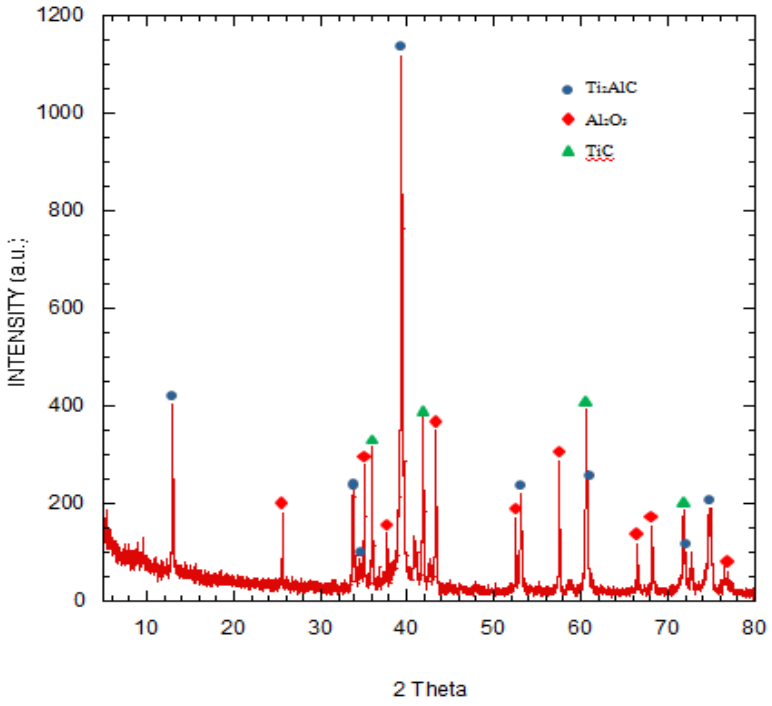

(b)

Figure 34. XRD patterns of the samples (a) PS9 (b) PS10.

Figure 34. shows the XRD patterns of PS9 and PS10 that were prepared using the same procedures but sintered at 1200 ^{o}C and 1400 ^{o}C, respectively. Mostly Ti_2AlC and Al_2O_3 with some TiC impurities were identified in the structure of pressureless sintered composites. In case of PS9 sintered at 1400 ℃, SiO_2 was also detected that came from the Nextel^{TM} 720 fiber. On the other hand, no SiO_2 was identified in PS10, which was sintered at 1400 ℃. This suggests that at 1400 ^{o}C, SiO_2 from the fibers most likely reacted with Ti_2AlC matrix, according to the reaction that was previously proposed in the literature [35].

SEM images of the sample PS9 pressureless sintered at 1200 ^{o}C are shown in Figure 35. Although, some of the Nextel^{TM} 720 fibers were broken during cold pressing and polishing, the fibers retained their shape after sintering, Figures 35 a and b. The dark gray areas in Figures 35 a and c are epoxy that permeated through pores during preparing sample for microscopy. The EDS result (Figure 35 c) shows that the Nextel^{TM} 720 fibers after pressureless sintering at 1200 ℃ still contain expected amount of SiO_2.

SEM images of the composite sample PS10 in Figure 36 show that Nextel^{TM} 720 decomposed and reacted with Ti_2AlC during sintering at 1400 ^{o}C Originally, Nextel^{TM} 720 fiber consists of 85 wt% of Al_2O_3 and 15 wt% of SiO_2. However, no SiO_2 was not detected at spot 1 in the fibers after sintering (Figure 36 c). Instead, about 24 % Si was identified in the Ti_2AlC, close to the alumina fiber - spots 2 and 4 in Figure 36 c. Far away from the alumina fiber (spot 3 in Figure 36 c) pure Ti_2AlC was detected. These results are in good agreement with XRD data sown in Figure 34, and once again confirm

that SiO_2 from the fibers reacts with Ti_2AlC at 1400 ^oC and probably forms $Ti_2Al_xSi_{1-x}C$ solid solution.

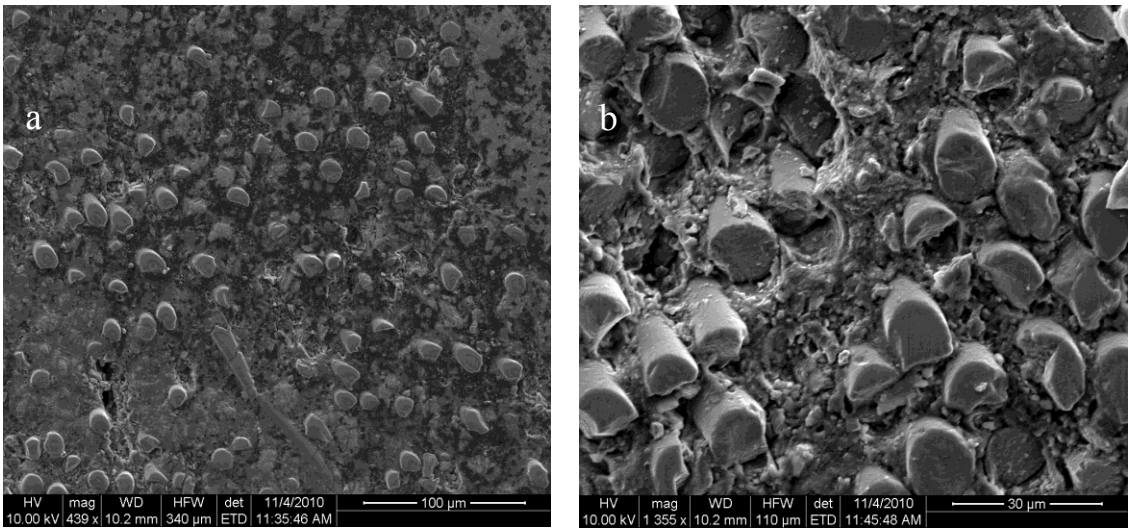

Spot	Al	O	C	Ti	Si	Major Phase
1	23.06	46.87	25.59	0.13	4.35	Al_2O_3 SiO_2
# Atomic %						

Figure 35. SEM images of composite sample PS9. (a) and (b) – Secondary Electron Image (c) Backscatter image with EDS results.

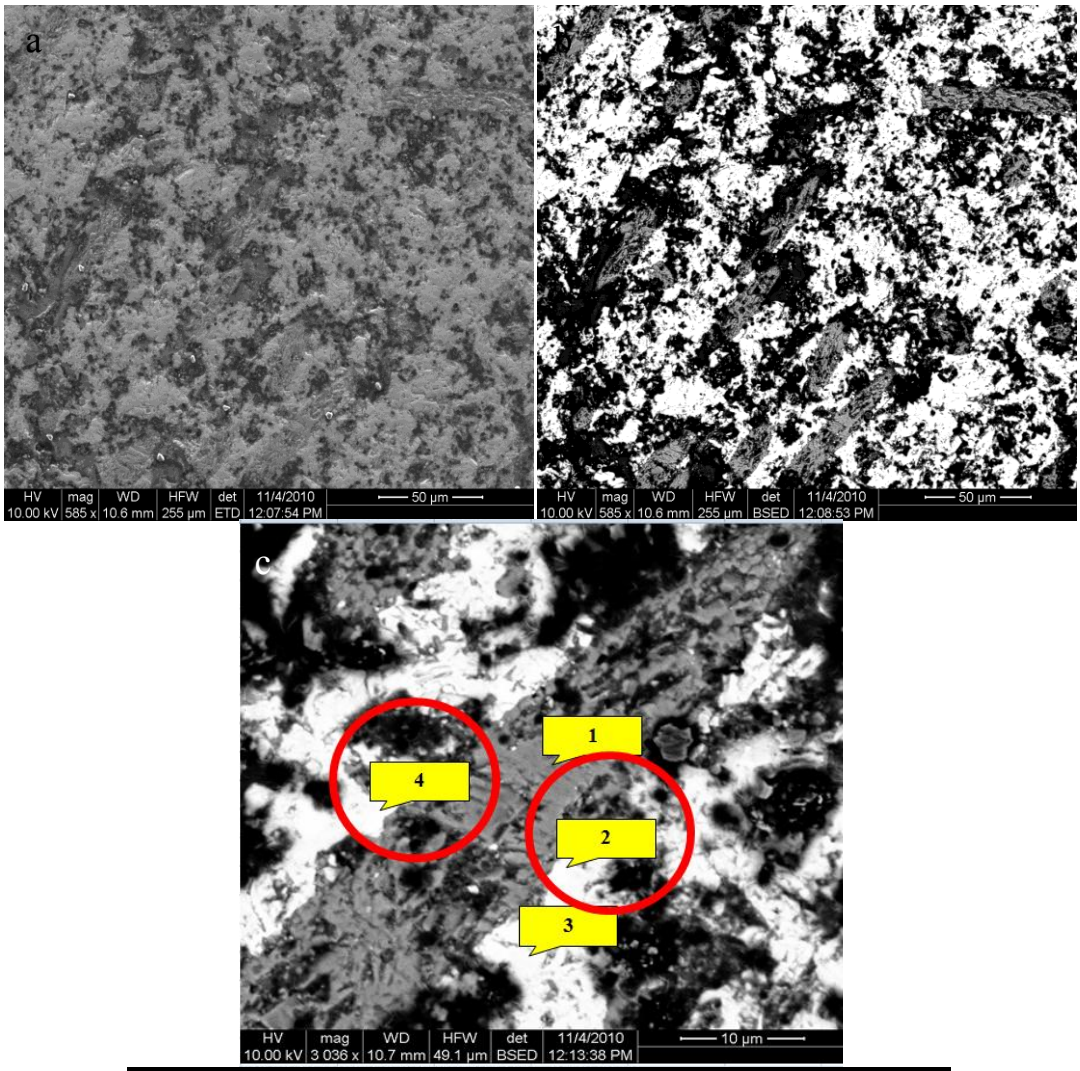

Spot	Al	O	C	Ti	Si	Major Phase
1	31.83	52.25	15.11	0.2	0.61	Al_2O_3
2	4.08	3.61	26.16	42.06	24.1	React
3	19.43	1.2	37.5	41.34	0.52	Ti_2AlC
4	3.77	5.89	21.53	45.04	23.76	React
# Atomic %						

Figure 36. SEM images of composite sample PS10. (a) Secondary Electron Image (b) and (c) Backscatter images with EDS results.

From the result of the pressureless sintering, it is clear that cold pressing of the powders and sintering temperatures at or above 1400 ^{o}C are required to pressureless sinter pure Ti_2AlC samples of high relative density. However, pressureless sintering is not appropriate to make high density composites with alumina fibers. It was found that alumina fibers hinder densification of Ti_2AlC during pressureless sintering, and thus higher sintering temperatures are required to process fully dense composts. However, at temperatures of 1400 ^{o}C alumina fibers decompose and SiO_2 from the fibers reacts with Ti_2AlC. Thus, in order to make high density composites at low temperature, Hot Isotatic Pressing (HIP) is needed. The major advantage of HIP is that HIPed materials have high density compared to the samples processed using other methods due to application of high isotropic pressure during sintering at temperature well below the melting point of the material.

3.4 Hot Isotatic Pressing (HIP)

The compositions, processing conditions and relative densities of the HIPed samples are listed in Table 14. It is obvious that the samples that were prepared by HIPing, have higher relative densities than pressureless sitered samples (Tables 12 and 13). H1 was prepared from pure Ti_2AlC powders without slip casting and had relative density of 96.2 %. H2 and H3 were prepared by slip casting mixture of Ti_2AlC powders and Nextel^{TM} 720 or ALBF1 fibers, respectively and they had relative densities of 97.6 and 92.0 %, respectively. The density of H3 was relatively lower than the other two

samples. This is because there were more fibers in H3 than H2 due to smaller diameter (3 um) of ALBF1 fibers when compared to Nextel^{TM} 720 (10 um), even though the samples were fabricated with same vol% of the fibers. This once again suggests that even in HIPing alumina fibers hinder densification of the composite samples.

Table 14. The relative densities of the HIPed samples.

Sample	Material	Process	Particle Size (um)	HIPing Pressure (MPa)	HIPing time and Temperature	**Relative Density**
H1	Ti_2AlC	-	-32	100	4 hours at 1300 °C	**96.2**
H2	Ti_2AlC+ 5vol% 720	Slip casting with 2dwb%PAA, and pH=4	-32	100	4 hours at 1300 °C	**97.6**
H3	Ti_2AlC+ 5vol% ALBF1	Slip casting with 2dwb%PAA, and pH=4	-32	100	4 hours at 1300 °C	**92.0**

Figure 37. shows the XRD pattern of the sample H1 processed by HIPing pure Ti_2AlC powders at 1300 ℃ under 100 MPa. Only two distinct phases can be identified: Ti_2AlC and TiC from initial powders after HIPing. SEM images and EDS result for H1 are shown in Figure 38. As the density of the sample increased through HIPing, the porosity of the sample definitely decreased compared to the pressureless sintering samples. Some etched SEM images are also shown in Figures 38 a and b illustrating polycrystalline structure of the HIPed samples. Selected but typical result of EDS analysis (spot 1 in Figure 38 c) shows the presence of Ti_2AlC. This result corresponds to

XRD result in Figure 37. It is apparent that no reaction or decomposition was detected while pure Ti_2AlC powder was HIPed at 1300 ℃ under 100 MPa.

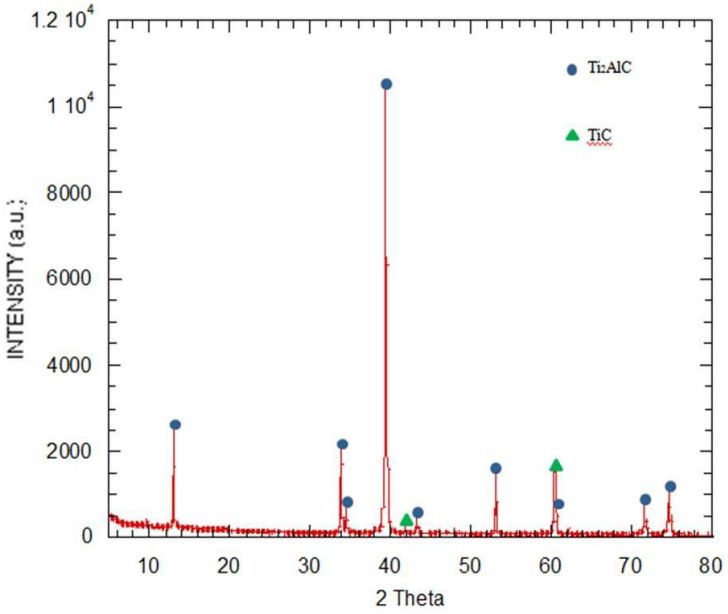

Figure 37. XRD pattern of H1.

Figure 39. shows the XRD pattern of the sample H2 processed by slip casting and HIPing the mixture of Ti_2AlC powders and Nextel^{TM} 720 fibers at 1300 ℃ under 100 MPa. Three distinct phases can be identified, Ti_2AlC, Al_2O_3, and TiC. Once again TiC present in the processed samples comes from the initial powders. No presence of SiO_2 can be detected by XRD. SEM images and EDS results for sample H2 are shown in Figure 40. It is clear that the Nextel^{TM} 720 fibers were evenly dispersed throughout the sample. And that they retain their shape after sintering. EDS results in spot 1 in Figure 40 c, shows presence of pure Ti_2AlC However, the composition in spot 2 and 3 (Figure

39 c) suggests that fibers consists of Al_2O_3 and SiO_2. However, SiO_2 content in Nextel^{TM}720 fibers was lower than expected. This suggests that some of SiO_2 probably reacted with Ti_2AlC during densification, but not so much as in the case of pressureless sintering at 1400 ^{o}C (Figure 36).

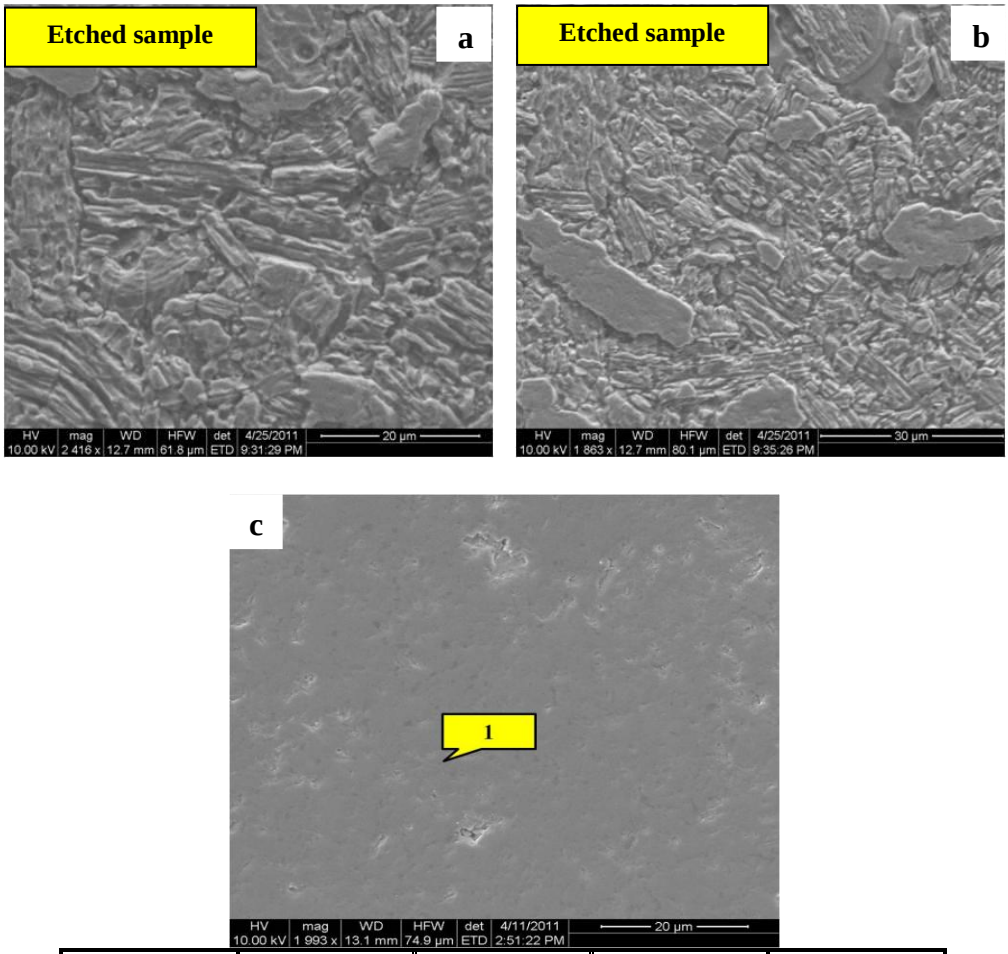

Spot	Al	C	Ti	Major Phase
1	22.15	33.23	42.62	Ti_2AlC
# Atomic %				

Figure 38. SEM image and EDS result of H1.

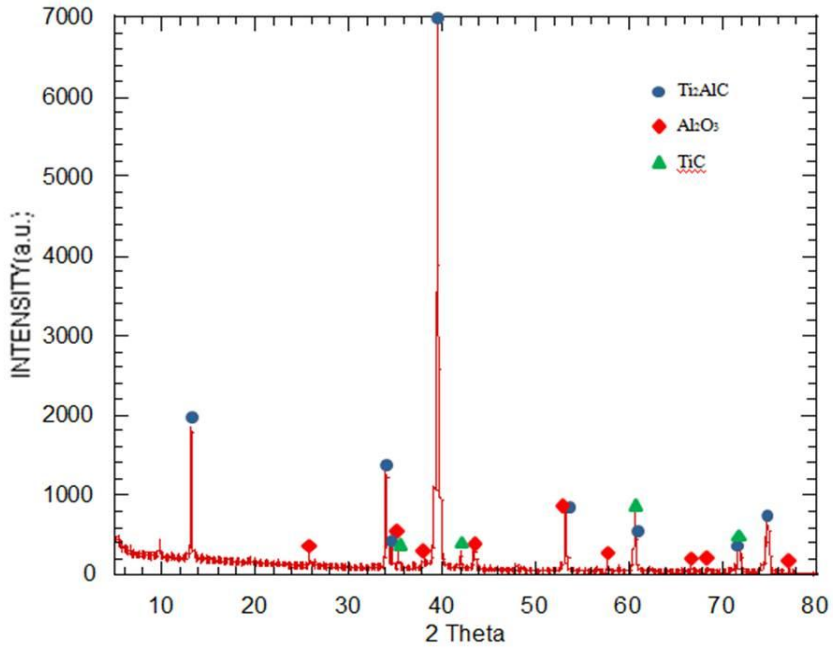

Figure 39. XRD pattern of H2.

Figure 41. shows the XRD pattern of the sample H3 processed by slip casting and HIPing the mixture of Ti_2AlC powders and ALBF1 fibers at 1300 ℃ under 100 MPa. Three distinct phases can be identified in the XRD pattern: Ti_2AlC, Al_2O_3, and TiC. The XRD patterns of H2 and H3 are very similar. SEM images and EDS results of the sample H3 are shown in Figure 42. More porosity were found because the density of H3 is lowest among the HIPed samples. However, the fibers are again evenly dispersed and retained their shape after sintering. EDS analysis in spot 1 and 2 (Figure 42 d) shows presence of, Ti_2AlC. In spot 3 (Figure 41d), Al_2O_3 and SiO_2 were identified. However, SiO_2 content in ALBF1 720 fibers was lower than expected. This result also suggests that some of SiO_2 possibly reacted with Ti_2AlC during densification.

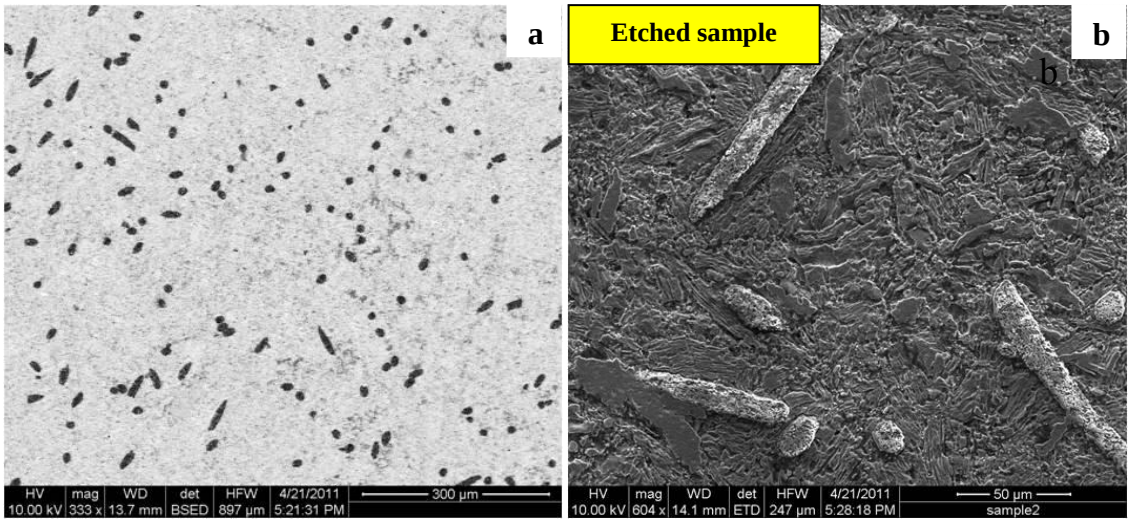

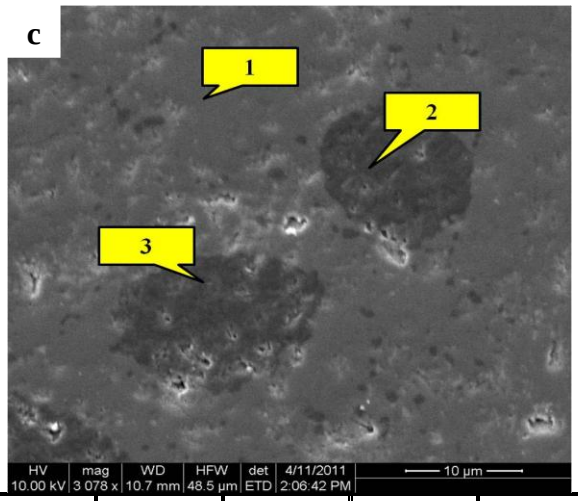

Spot	Al	O	C	Ti	Si	Major Phase
1	21.72	-	30.91	47.37	-	Ti_2AlC
2	42.62	55.29	-	-	2.09	Al_2O_3 SiO_2
3	45.65	53.38	-	-	0.96	Al_2O_3
# Atomic %						

Figure 40. SEM images and EDS results of H2.

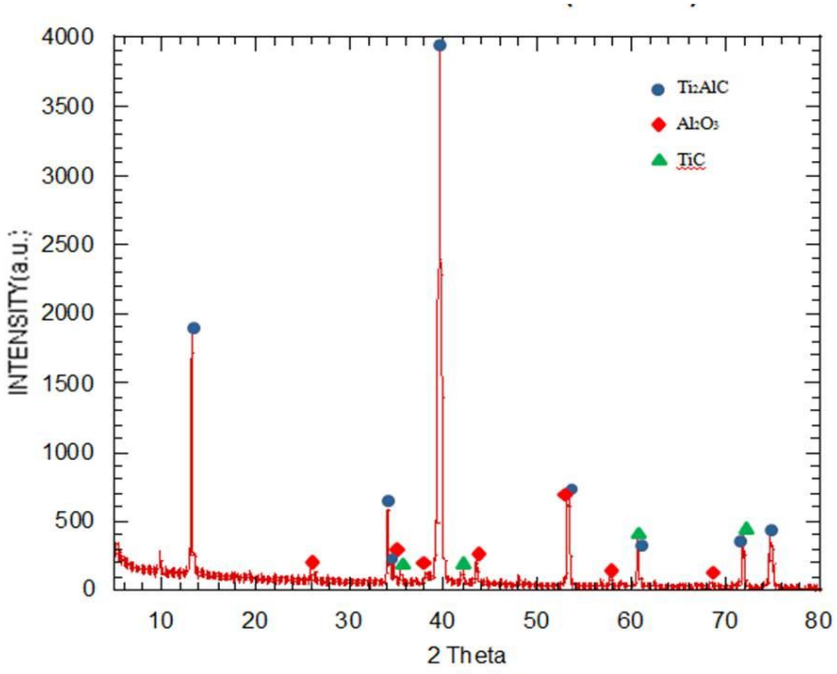

Figure 41. XRD pattern of the sample H3.

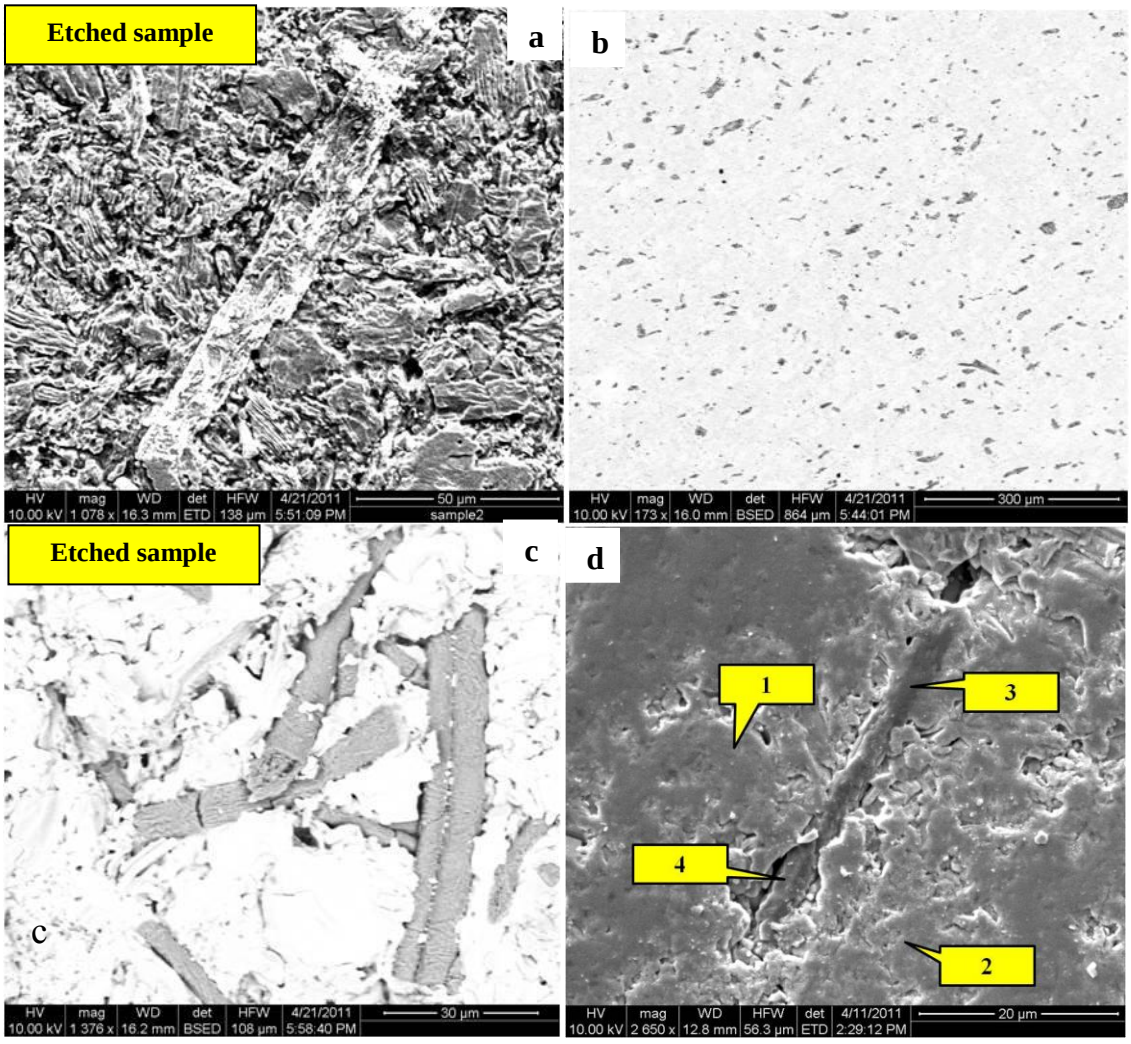

Spot	Al	O	C	Ti	Si	Major Phase
1	21.57	-	33.53	44.90	-	Ti_2AlC
2	22.71	-	31.34	45.95	-	Ti_2AlC
3	35.99	61.81	-	-	2.19	Al_2O_3 SiO_2
4	37.96	61.32	-	-	0.72	Al_2O_3
# Atomic %						

Figure 42. SEM images and EDS results of H3.

3.5 Mechanical Characterization

Vickers hardness was measured 5 times on each sample at different locations. Vickers hardness of the HIPed samples is shown in Table 15 and Figure 43. The Vickers hardness of H1, which was pure Ti_2AlC material, was 3.63 GPa. This result is in good agreement with previously published data for fully dense Ti_2AlC of 4.5 [2] and 2.8 [17],

Table 15. Vickers hardness of the HIPed samples.

Sample	Average	Standard Deviation	1	2	3	4	5
H1 (GPa)	3.63	0.394	3.15	3.43	3.51	4.01	4.07
H2 (GPa)	4.36	0.259	3.97	4.25	4.47	4.48	4.64
H3 (GPa)	2.98	0.151	2.81	2.93	2.93	3.00	3.22

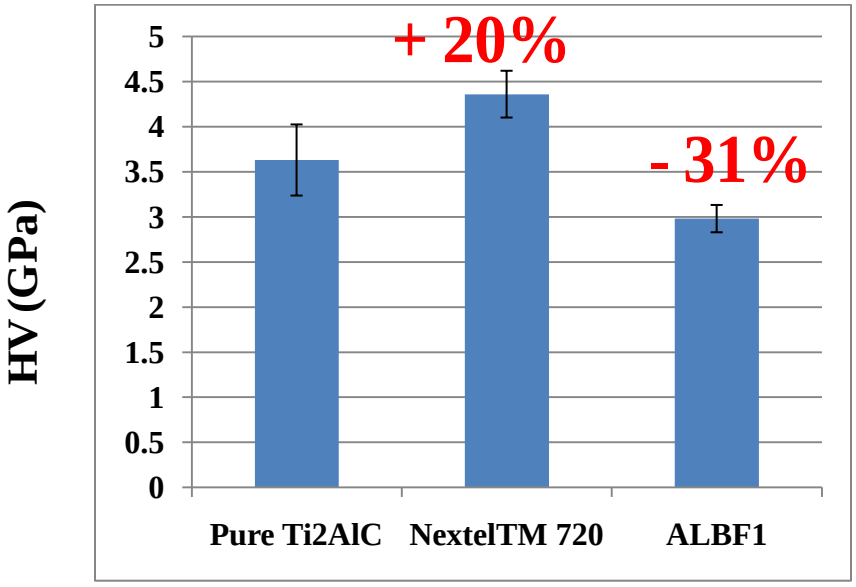

Figure 43. Results of the Vickers hardness measurements.

The Vickers hardness of H2, which was reinforced with 5 vol% Nextel^{TM} 720, was higher for about 20 % than that of H1. It is clear that the Nextel^{TM} 720 fibers enhance the Vickers hardness of the sample. On the other hand, the Vickers hardness of H2, which was reinforced with 5 vol% ALBF1, decreased by about 31 % when compared to H1. The relatively low density of the H3 could be the main reason for its low Vickers hardness.

Table 16. Elastic moduli of the samples.

Sample	Young's modulus (GPa)	Shear modulus (GPa)	Poison's ratio
H1	249.3	106.1	0.175
H2	256.4	109.7	0.169
H3	212.0	90.3	0.174

Elastic moduli (Young's modulus, E, and shear modulus, G, and poison's ratio, v) of the samples are shown in Table 16. The Elastic moduli of H1, which was pure Ti_2AlC material, were 249.3 GPa (E) and 106.1 GPa (G) respectively and those results are in good agreement with previously published data [25]. The Elastic moduli of H2, which was reinforced with 5 vol% Nextel^{TM} 720, increased by about 3 % compared to H1. As expected, that the Nextel^{TM} 720 fibers enhance the Elastic moduli of the sample since alumina has higher elastic moduls than Ti_2AlC. On the other hand, the Elastic moduli of H2, which was reinforced with 5 vol% ALBF1, decreased by about 15 % when compared to H1. The relatively low density of the H3 is also the main reason for low Elastic moduli measured for sample H3.

Fracture toughness (K_{1C}) of the samples determined by double torsion are shown in Table 17 and summarized in Figure 44. The precrack sizes of the HIPed samples were measured by the optical microscope. The average fracture toughness of H1, which was pure Ti_2AlC material, was 8.34 $MPa \cdot m^{1/2}$, slightly above previously published value of 6.5 $MPa \cdot m^{1/2}$ [17] and 7.1 $MPa \cdot m^{1/2}$ [31]. The fracture toughness of H2, which was reinforced with 5 vol% Nextel^{TM} 720, increased by about 8.6 % when compared to the pure Ti_2AlC (sample H1). It is clear that addition of evenly dispersed Nextel^{TM} 720 fibers enhance the fracture toughness of Ti_2AlC. On the other hand, the fracture toughness of H2, which was reinforced with 5 vol% ALBF1, decreased by about 12 % compared to H1, i.e. pure Ti_2AlC. Once again, the relatively low density of the H3 could be also the main reason for its low fracture toughness.

Table 17. The values of K_{1C} of the HIPed samples.

Sample		Precrack Size (um)	Thickness (mm)	Critical load (N)	K_{1C} (MPa$\sqrt{m}$)
Pure Ti_2AlC (H1)	1	174.6	10.140	92.204	8.614
	2	241.74	1.0048	93.895	8.929
	3	896.93	1.0104	91.047	8.564
	4	1206.02	1.0145	84.238	7.862
	5	1896.29	1.0089	81.969	7.733
	Average K_{1C} : 8.34 MPa·$m^{1/2}$, Standard Deviation : 0.517				
5vol% Nextel™ 720 composite (H2)	1	150.4	1.0063	93.895	8.880
	2	407.38	1.0023	94.740	9.032
	3	515.43	1.0038	104.397	9.922
	4	940.34	1.0180	93.405	8.635
	5	1050.04	1.0135	91.981	8.579
	6	1120.33	1.0099	98.790	9.278
	Average K_{1C} : 9.055 MPa·$m^{1/2}$, Standard Deviation : 0.497				
5vol% ALBF1 composite (H3)	1	762.35	1.0160	79.210	7.368
	2	1467.38	1.0068	99.146	9.387
	3	1475.91	1.0190	55.447	5.127
	4	4934.93	1.0094	78.587	7.404
	Average K_{1C} : 7.321 MPa·$m^{1/2}$, Standard Deviation : 1.7409				

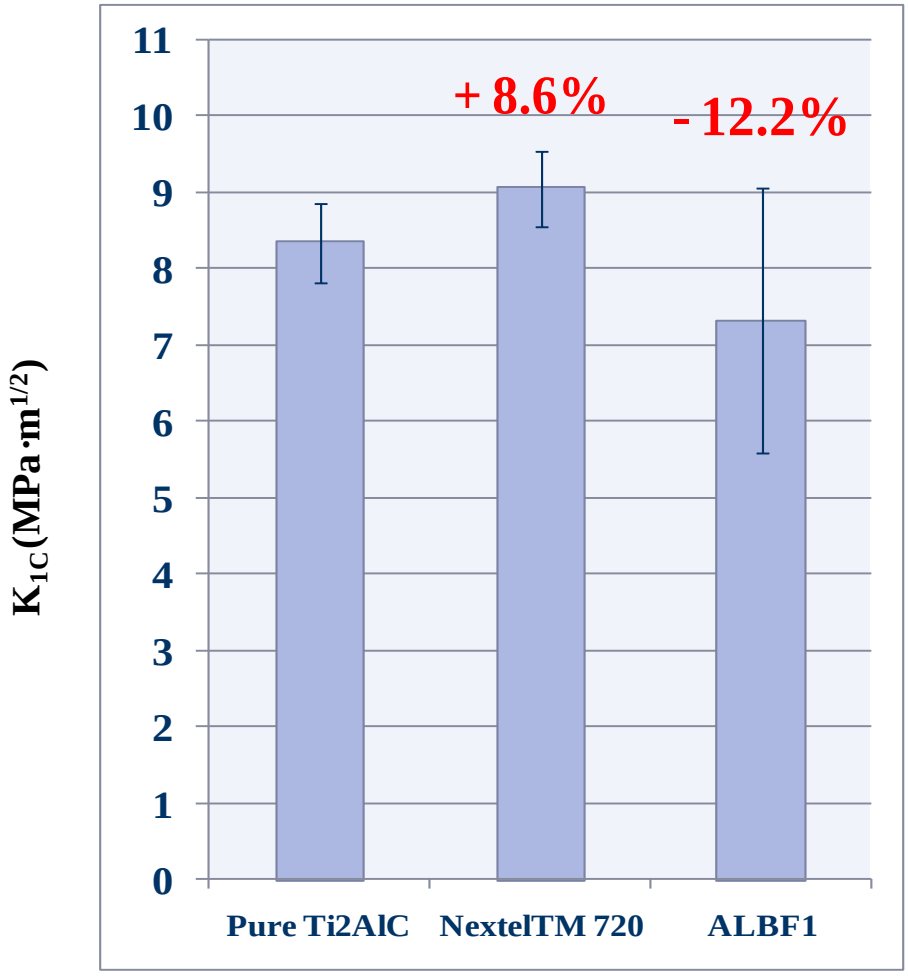

Figure 44. Fracture toughness of the HIPed samples.

The BSE and SEM images of the samples' precracks are shown in Figure 45. The cracks were deflected at the grain boundaries in pure Ti_2AlC. However, in composite samples (Figures 45 b and c), large crack deflections can be also observed at the fiber/matrix interfaces. These crack deflections is one of the mechanisms that enhance the fracture toughness of the samples.

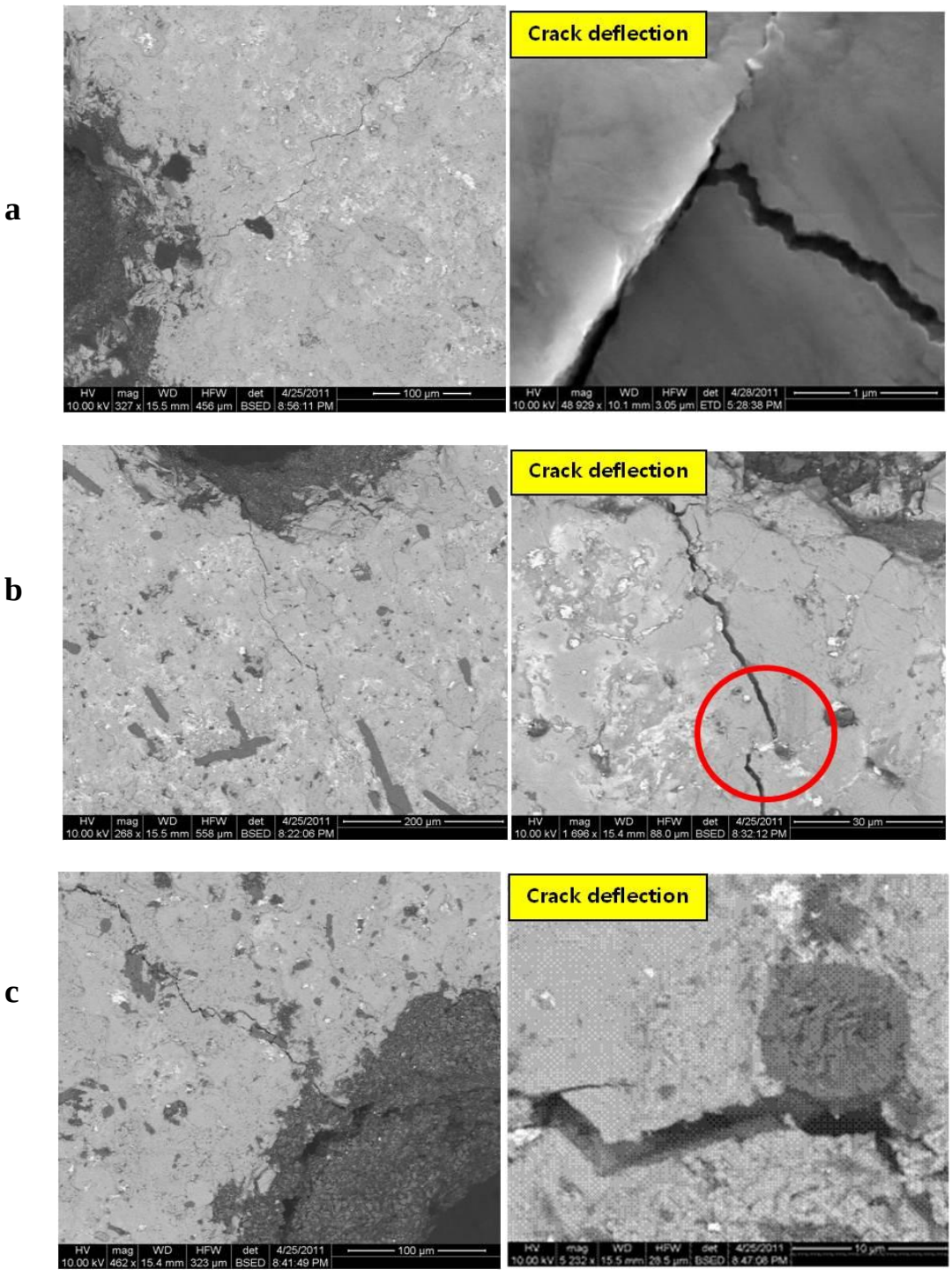

Figure 45. BSE and SEM images of the precrack (a) Pure Ti_2AlC (b) Nextel^{TM} 720 composite (c) ALBF1 composite.

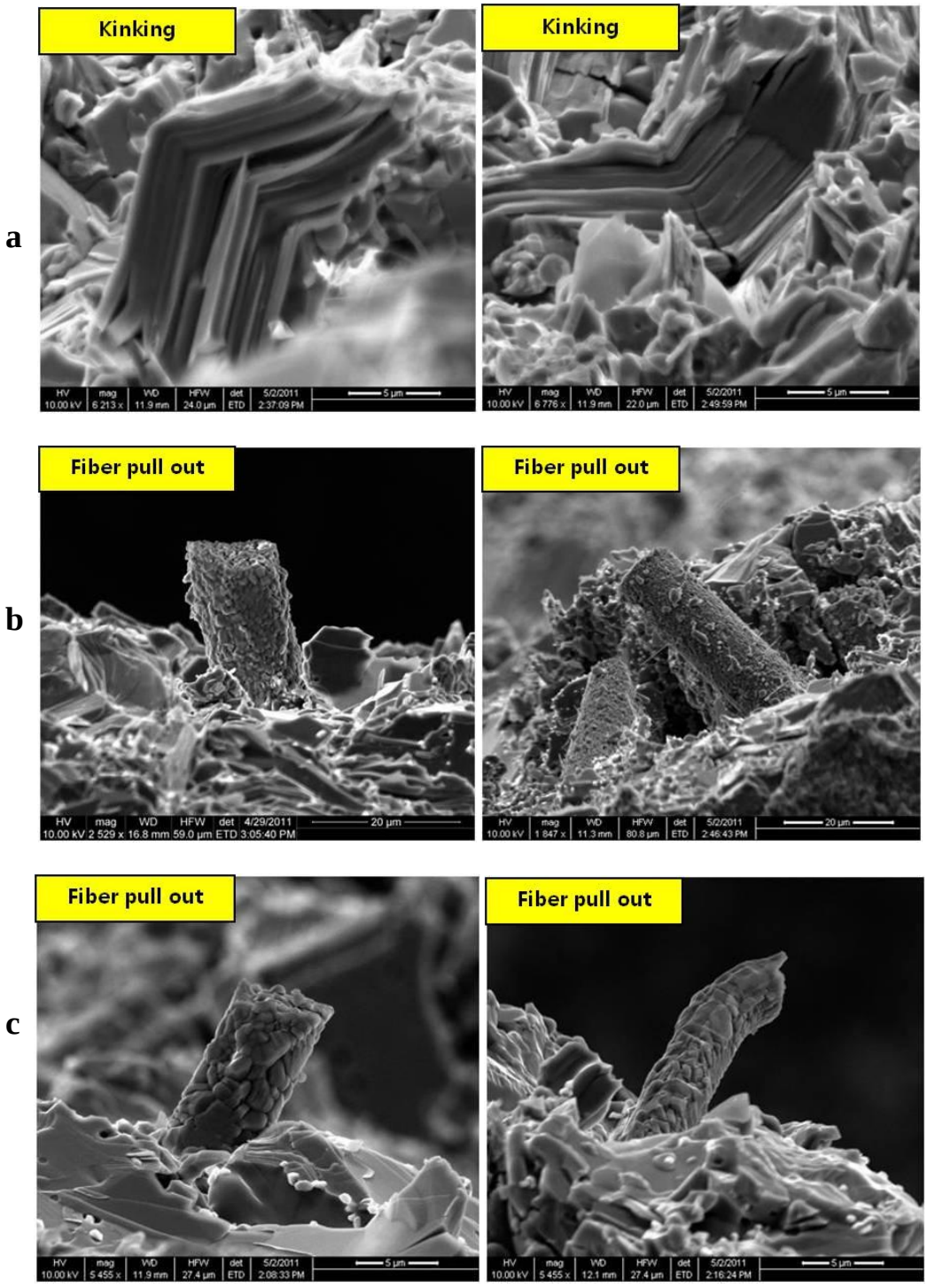

Figure 46. BSE and SEM images of the fracture surface (a) pure Ti_2AlC (b) Nextel^{TM} 720 composite (c) ALBF1 composite.

The SEM images of the samples' fracture surfaces are shown in Figure 46. The typical deformation of the MAX phases, such as delaminations and kinking, are clearly observed in the pure Ti_2AlC samples. As it was mentioned before (see Section 1.2), kinking and delamination are considered to be the main reason for high fracture toughness of Ti_2AlC when compared to other monolithic ceramics. In case the composites reinforced with alumina fibers (Figures 46 b and c), beside kinking and crack deflection, fiber pull outs can be also observed. The fibers pull outs are the main toughening mechanisms in fiber reinforced composites, and as it clearly shown in Figures 46 b and c, it takes place in the alumina fiber reinforced Ti_2AlC composites. These pulled out of the fibers enhance the fracture toughness of the Ti_2AlC samples, as it is shown in the case of sample H2 (Table 17 and Figure 44) that was reinforced with Nextel^{TM} 720 fibers**.** However, the overall fracture toughness of the samples H3 reinforced with ALBF1 fibers is lower than that of the pure Ti_2AlC (Table 17 and Figure 44). This is not because crack deflection and fiber pull outs as toughening mechanisms are not present in that sample, but rather because of low relative density of this composite material.

4. SUMMARY AND CONCLUSION

Homogeneous dispersion of the Nextel^{TM} 720 and ALBF1 in Ti_2AlC without fiber agglomeration can be achieved by slip casting fibers and powders previously dispersed in aqueous solutions with PAA and pH=4. It was found that suspensions prepared with 2 dwb% PAA as a dispersant and has an excellent stability in the pH range of 4 ~ 5.

Composite green bodies were densified by pressureless sintering or HIPing at different temperatures. Although Ti_2AlC can be pressureless sintered to high relative density at 1400 ^oC, addition of alumina fibers in the composites hinders densification. Therefore, alumina fiber reinforced Ti_2AlC cannot be fully densified using pressureless sintering. In addition, sintering temperature should be below 1400 ^oC because SiO_2 in alumina fibers reacts with Ti_2AlC. It was found that HIPing at 1300 ^oC for 4 hours at 100 MPa results in almost fully dense composites with majority phases being alumina fibers and Ti_2AlC.

The double torsion (DT) tests were carried out at room temperature to measure the fracture toughness of the HIPed pure and 5 vol% alumina fiber reinforced Ti_2AlC. Moderate increase in fracture toughness of ~ 9 % was measured for Ti_2AlC reinforced with only 5 vol% Nextel^{TM} 720. SEM study of the fracture surfaces after DT tests showed toughening mechanisms, such as crack bridging, crack deflection and fiber pull-outs, are responsible for observed increase in fracture toughness. However, fracture toughness of the samples reinforced with ALBF1 was lower than that of pure Ti_2AlC

because of the low relative densities of those composites. High residual porosity in composites (Ti_2AlC + ALBF1) is responsible for significant decrease in fracture toughness regardless of operative toughening mechanisms.

Elastic moduli and Vickers hardness of HIPed Ti_2AlC were measured by Resonant Ultrasound Spectroscopy (RUS) and Microhardness Tester respectively. In case of elastic moduli, no significant change was found due to reinforcement with alumina fibers. On the other hand, Vickers hardness of composites was found to be larger for Ti_2AlC reinforced with Nextel^{TM} 720 and lower for the samples reinforced with ALBF1 due to the low relative density.

Results of this study suggest that fracture of Ti_2AlC can be toughened by addition of Al_2O_3 fibers, such as Nextel^{TM} 720 and ALBF1, if sintering temperature is kept at, or below 1300 ^{o}C and processed composites are almost fully dense. However, to exploit the benefits of toughening Ti_2AlC with alumina fibers, larger volume fractions of the fibers (more than 5 vol%) have to be used to processed Al_2O_3 fiber reinforced Ti_2AlC composites.

REFERENCES

1. M.W. Barsoum and T. El-Raghy, *American Scientist*, 2001, **89,** 334-343.
2. M.W. Barsoum, *Progress in Solid State Chemistry*, 2000, **28,** 201-281.
3. M.W. Barsoum, *Encyclopedia of Materials: Science and Technology*, eds. K.H.J. Buschow, Elsevier, Amsterdam, NY, 2006, 11, 1-11.
4. W. Jeitschk and H. Nowotny, *Monatshefte Fur Chemie*, 1967, **98**, 329
5. H. Wolfsgru, H. Nowotny, and F. Benesovs, *Monatshefte Fur Chemie*, 1967, **98,** 2403.
6. S. Dubois, T. Cabioch, P. Chartier, V. Gauthier, and M. Jaouen, *Journal of the American Ceramic Society*, 2007, **90**, 2642-2644.
7. J. Etzkorn, M. Ade, and H. Hillebrecht, *Inorganic Chemistry*, 2007, **46**, 1410-1418.
8. C.F. Hu, F. Li, J. Zhang, J. Wang, and Y. Zhou, *Scripta Materialia*, 2007, **57**, 893-896.
9. C.F. Hu, J. Zhang, J. Wang, F. Li, and Y. Zhou, *Journal of the American Ceramic Society*, 2008, **91,** 636-639.
10. C.L. Li, J. Kuo, B. Wang, Y. Li, and R. Wang, *Journal of Physics D-Applied Physics*, 2009, **42**, 75404-75408.
11. A.T. Procopio, T. El-Raghy, and M.W. Barsoum, *Metallurgical and Materials Transactions a-Physical Metallurgy and Materials Science*, 2000, **31**, 373-378.

12. Y.L. Bai, X. He, Y. Li, C. Zhu, and M. Li, *Solid State Communications*, 2009, **149**, 2156-2159.

13. M.W. Barsoum, *Encyclopedia of Materials: Science and Technology*, eds. K.H.J. Buschow, Elsevier, Amsterdam, NY, 2004, 11, 1-16.

14. W. Jeitschko, H. Nowotny, and F. Benesovsky, *Monatshefte Fur Chemie*, 1963, **94**, 672.

15. V.I. Ivchenko, V.F. Nemechenko, and T.Y. Kosolapova, *Powder Metall. Met. Ceram.*, 1976, **367**, 15.

16. M.W. Barsoum and T. El-Raghy, *Journal of Materials Synthesis and Processing*, 1997, **5**, 197-216.

17. M.W. Barsoum, M. Ali, and T. El-Raghy, *Metallurgical and Materials Transactions a-Physical Metallurgy and Materials Science*, 2000, **31**, 1857-1865.

18. B.C. Mei, W. Zhou, and X. Hong, *Journal of Materials Science*, 2004, **39,** 1471-1472.

19. Y. Khoptiar, I. Gotman, and E.Y. Gutmanas, *Journal of the American Ceramic Society*, 2005, **88**, 28-33.

20. X.H. Wang and Y.C. Zhou, *Journal of Materials Science & Technology*, 2010, **26**, 385-416.

21. M.W. Barsoum, *Journal of the Electrochemical Society*, 2001, **148**, 544-550.

22. M. Sundberg, G. Malmgvis, A. Magnusson, and T. El-Raghy, *Ceramics International*, 2004, **30**, 1899-1904.

23. J.W. Byeon, J. Liu, M. Hopkins, N. Garimella, and M. Radovic, *Oxidation of Metals*, 2007, **68**, 97-111.

24. A.G. Zhou and M.W. Barsoum, *Journal of Alloys and Compounds*, 2010, **498**, 62-70.

25. P. Finkel, M.W. Barsoum, and T. El-Raghy, *Journal of Applied Physics*, 2000, **87**, 1701-1703.

26. C.J. Gilbert, D.R. Bloyer, M.W. Barsoum, T. El-Raghy, A.P. Tomsial, and R.O. Ritchiel, *Scripta Materialia*, 2000, **42**, 761-767.

27. S.B. Hashimoto, M. Takeuchi, S. Honda, H. Awaji, and S. Zhang, *Materials Letters*, 2008, **62**, 1480-1483.

28. D.L. Zhang, Z.H. Cai, A.J. Huang, and R. Yang, *Journal of the American Ceramic Society*, 2006, **89**, 3325-3330.

29. M.W. Barsoum, D. Brodkin, and T. El-Raghy, *Scripta Materialia*, 1997, **36,** 535-541.

30. P. Wang, B. Mei, X. Hong, and W. Zhou, *Transactions of Nonferrous Metals Society of China*, 2007, **17,** 1001-1004.

31. J.X. Chen and Y.C. Zhou, *Scripta Materialia*, 2004, **50**, 897-901.

32. F.L. Meng, Y.C. Zhou, and J.Y. Wang, *Scripta Materialia*, 2005,**53**,1369-1372.

33. K.G. Dassios, M. Steen, and C. Filiou, *Materials Science and Engineering A*, 2003, **349**, 63-72.

34. C.B. Spencer, J.M. Córdobad, N. Obando, A. Sakulich, M. Radovic, M. Odénc, L. Hultman, and M.W. Barsoum, *Journal of the American Ceramic Society*, 2011, **94**, 1551.

35. C.B. Spencer, J.M. Córdobad, N. Obando, A. Sakulich, M. Radovic, M. Odénc, L. Hultman, and M.W. Barsoum, *Journal of the American Ceramic Society*, 2011, **94**, 2916.

36. K.G. Dassios, M. Steen, and C. Filiou, *Materials Science and Engineering A*, 2003, **349**, 63-72.

37. D.M. Wilson, S.L. Lieder, and D.C. Lueneburg, *Ceramic Engineering and Science Proceedings*. 2008, **16**, 1005-1014.

38. F. Deleglise, M.H. Berger, and A.R. Bunsell, *Journal of the European Ceramic Society*, 2001, **21**, 569-580.

39. Z. Sun, M. Li, M. Hu, and Y. Zhou, *Journal of the American Ceramic Society*, 2009, **92**, 1695-1702.

40. J.A. Lewis, *Journal of the American Ceramic Society*, 2000, **83**, 2341-2359.

41. A. Murugaiah, A. Souchet, T. El-Raghy, M. Radovic, and M. Sundberg, *Journal of the American Ceramic Society*, 2004, **87**, 550-556.

42. J.O. Outwater and D.J. Gerry, *Journal of Adhesion*, 1969, **1**, 290.

43. M. Radovic and E. Lara-Curzio, *Acta Materialia*, 2004, **52**, 5747-5756.

44. M. Radovic, E. Lara-Curzio, and G. Nelson, *Ceramic Engineering and Science Proceedings*, 2008, **27**, 63-73.

VITA

Name:	Kwonguk Jeon
Address:	Texas A&M University, Department of Mechanical Engineering, 3123 TAMU, College Station, TX 77843-3123
Email Address:	kwongukjeon@gmail.com
Education:	B.E., Weapons Engineering, Korea Military Academy in South Korea, 2001
	M.S., Mechanical Engineering, Texas A&M University, 2011